AD NUMBER

AD910866

NEW LIMITATION CHANGE

TO

Approved for public release, distribution unlimited

FROM

Distribution authorized to U.S. Gov't. agencies only; Test and Evaluation; MAY 1973. Other requests shall be referred to Air Force Avionics Lab., AFSC, Wright-Patterson AFB, OH 45433.

AUTHORITY

AFAL ltr, May 1973

AFAL-TR-73-176

IMPROVED LARGE ZnS WINDOWS

B. A. diBenedetto
J. Pappis
A. J. Capriulo

Raytheon Company
Waltham, Massachusetts

TECHNICAL REPORT AFAL-TR-73-176
MAY 1973

Air Force Avionics Laboratory
Air Force Systems Command
Wright-Patterson Air Force Base, Ohio 45433

NOTICE

When Government drawings, specifications, or other data are used for any purpose other than in connection with a definitely related Government procurement operation, the United States Government thereby incurs no responsibility nor any obligation whatsoever; and the fact that the government may have formulated, furnished, or in any way supplied the said drawings, specifications, or other data, is not to be regarded by implication or otherwise as in any manner licensing the holder or any other person or corporation, or conveying any rights or permission to manufacture, use, or sell any patented invention that may in any way be related thereto.

Copies of this report should not be returned unless return is required by security considerations, contractual obligations, or notice on a specific document.

IMPROVED LARGE ZnS WINDOWS

B. A. diBenedetto
J. Pappis
A. J. Capriulo

FOREWORD

This report was prepared by Raytheon Company, Research Division, Waltham, Mass., under Contract No. F33615-73-C-1048, Project No. 6102, entitled, "Improved Large ZnS Windows," The work was administered under the direction of the Air Force Avionics Laboratory, Wright-Patterson Air Force Base, Ohio. Mr. C. T. Ennis (TEL) was task engineer.

At Raytheon, the investigation was carried on in the Advanced Materials Department of the Research Division. Dr. J. Pappis Department Manager, and Mr. B. A. diBenedetto, principal investigator.

This is the Final Technical Report for Contract F33615-73-C-1048. It covers the period August 1972 to January 1973. The report was given the Raytheon internal number S-1559.

This report was submitted by the authors April 1973.

This technical report has been reviewed and is approved.

ROBERT E. DEAL, Chief
Laser & E-O Technology Branch
Electronic Technology Division

ABSTRACT

The significance of this research and development program to the Air Force is the demonstrated feasibility of fabricating large infrared transmitting windows of zinc sulfide with good physical and optical characteristics by the chemical vapor deposition process. Plates approximately 1 ft. × 2 ft. with good transmitting properties in the 8 - 12 μm band were made and samples from these plates were submitted to the Air Force Avionics Laboratory for further evaluation.

Three major accomplishments of the program were: the elimination of visible-to-the-eye zinc inclusions, the elimination of plate fracture during cooldown from the deposition temperature, and the improvement of the as-deposited thickness profile. As a result of these improvements the cost of window blanks can be significantly reduced.

Interferometric measurements on samples taken from typical deposits indicate that diffraction limited imaging can be expected at all infrared wavelengths and that even at 0.9 μm image degradation is still slight. Angular resolution at all wavelengths will be degraded less than 10 μradians by transmission through 1 centimeter of the material, and is adequate for all known infrared systems applications. The main problem with the use of this material is in the overall signal reduction due to residual scatter, and in the increased background levels that will degrade the performance of systems designed not for thermal sensing but for active i. r. or passive sensing at wavelengths in the visible and near i. r. wavelength range. The latter uses will also be affected by the extrinsic absorption band between 0.4 and 0.9 μm. Improvement of the material for these applications may possibly be accomplished by the use of aliovalent additives as well as by the use of additives that suppress the formation of scattering sites.

TABLE OF CONTENTS

LIST OF ILLUSTRATIONS

LIST OF ILLUSTRATIONS (Cont'd)

SECTION I
INTRODUCTION

Reconnaissance and weapon delivery applications require infrared windows that can be fabricated into large sizes and various geometric shapes. For example, FLIR type applications require large size IR windows with good physical properties to withstand severe environmental conditions. For the past decade considerable effort has been devoted toward the development of suitable windows. Window blanks have been formed by special glass casting, hot pressing and crystal growth techniques, but none of the processes have yielded totally satisfactory windows. Another process that was explored under contracts F33615-70-C-1577 and F33615-71-C-1775, and found to yield good optical quality material is the chemical vapor deposition process. This process is not inherently size or shape limited, and it has the potential of fabricating good optical quality polycrystalline infrared transmitting material. The Air Force Avionics Laboratory, recognizing the potential of this process, continued the effort initiated under the original contracts to further develop zinc sulfide and to scale the process to fabricate large aperture infrared windows.

At the conclusion of the previous program it had been demonstrated that large plates (~13 × 20 × 1/2 in.) could be fabricated by the CVD process although the optical quality (scatter) of the material, particularly at visible wavelengths, was not as good as that observed in some of the experimental deposits. In an attempt to resolve this problem a six-month experimental program was conducted in which four problem areas were addressed. These were:

1) elimination of zinc inclusions
2) improved thickness distribution
3) improved operating procedures to eliminate or minimize "banding" in the material
4) elimination of plate fracture during cooldown.

The program was iterative in nature, in that we attempted to eliminate visible-to-the-eye inclusions and then addressed ourselves to improving the thickness profile as well as controlling the process parameters to eliminate or minimize bands in the thickness of the material. In addition, throughout the program, modifications were continually made in mandrel design to eliminate plate fracture during cooldown from the deposition temperature.

SECTION II
THE CHEMICAL VAPOR DEPOSITION PROCESS

The chemical vapor deposition (CVD) process offers many advantages over conventional techniques for preparing infrared transmitting materials. Perhaps the two most significant advantages are that the resulting material is very pure, thus eliminating IR absorptions due to impurities and that the deposits are usually very dense, and thus light scattering due to pores is minimized. Furthermore, the process is not inherently size limited and it has the potential of fabricating polycrystalline infrared windows in large sizes and various shapes.

The chemical vapor deposition process can be summarized as follows: Volatile compounds of the elements comprising the material to be deposited are reacted at a surface whose temperature allows the compound to decompose or react to form a solid, adherent coating. If the coating thickness is heavy enough a monolithic free-standing plate is obtained. The volatile byproducts of the reaction are pumped away, flushed away in a stream of carrier gas, removed by reaction with a mass of suitable material in the system, or regenerated or used by reaction with a reservoir of a suitable raw material.

Chemical vapor deposition processes can be used to form the most refractory substances at temperatures where their vapor pressure is negligible. The properties of the deposited materials can be significantly and controllably altered by the co-deposition of alloying atoms. Depending on the relative concentration of the reactants, either solid solutions or two-phase composites can be formed. Crystallite orientation and size distribution can be controlled by proper manipulation of the deposition parameters. Composites with alternating layers of two or more different materials can be prepared by cycling the composition of the vapors from which the materials are deposited.

Two general types of systems, static and dynamic, can be used for chemical vapor deposition. The static system is a closed system, in which the reactants and products are sealed in a chamber. Well-known examples are the quartz-iodine incandescent lamp and the hydro-thermal bomb for the deposition of synthetic quartz. In the dynamic system, on the other hand, fresh reactants are continuously metered into the deposition chamber, and the spent vapors are continuously removed, usually by pumping. The reactive gases are fed into the furnace through a gas-metering system. The substrate upon which the deposit occurs is maintained at an appropriate temperature by means of a heater that is inductively or resistively heated. Most vapor depositions are made at pressures on the order of one-hundredth of an atmosphere, although a much higher or lower pressure can be employed.

Our experiments have shown that the dynamic system yields good results in the deposition of zinc and cadmium sulfide and zinc selenide, and is perferable because it offers certain advantages. Chief among these is the depletion of reactants and the accumulation of waste materials which are major problems in the static system, are minimal in the dynamic system which allows the addition and removal of materials during deposition. In order to obtain a deposit, the temperature of the substrate chamber and the vapor source are usually more critical and interdependent in the static system than in the dynamic system. The static system, in general, offers less flexibility in the deposition parameters than the dynamic system, since vapor transport is controlled by temperature gradients rather than pressure gradients and mass flow. In addition, the static system is often more susceptible to vapor phase nucleation and particle growth near the substrate; to reduce this effect the partial pressures of the reactive vapors must be low, resulting in low deposition rates. The reactive vapor concentrations are also limited by the equilibrium constants of regenerative reactions and by the fact that partial pressures of the regenerative vapor cannot (for safety reasons) usually greatly exceed one atmosphere. Finally, outgassing of deposition chamber and substrate are of greater importance in the static system than in the dynamic system.

Two general techniques can be employed in vapor deposition. These are: 1) Conventional chemical vapor deposition where the vapor source temperature is lower than the substrate temperature; 2) Transport chemical vapor deposition, where the vapor source temperature is greater than the substrate temperature.

In conventional chemical vapor deposition, the thermodynamics and kinetics of the chemical reactions are such that formation of the solid product is favored at the higher temperatures, whereas the volatile reactants tend to be formed or are stable at the lower temperatures.

In chemical transport deposition, on the other hand, the thermodynamics and kinetics of the chemical reactions are such that formation of the solid product is favored at the lower temperatures, whereas the volatile reactants are formed at the higher temperatures.

The initial experiments at Raytheon employed chemical transport deposition in a dynamic system using HCl to transport zinc sulfide. It was soon discovered that conventional chemical vapor deposition in a dynamic system yielded superior results, and this method was used exclusively to fulfill the objectives of this program.

SECTION III
PROCESS RUNS

During the preceding contracts a process for the chemical vapor deposition of theoretically dense zinc sulfide had been established. Using this process several large plates had been deposited and submitted to the Air Force Avionics Laboratory for further evaluation. Analysis of the material at that time indicated that its optical quality could be improved, provided visible-to-the-eye zinc inclusions, small scattering sites, and "bands" in the thickness direction could be minimized or eliminated. (Bands are defined as layers of material that scatter more than material on either side of it.) Furthermore, to obtain usable window blanks from each run the thickness distribution needed improvement and random cracking of the deposits during cooldown had to be eliminated.

Based on previous process runs it was known that low scattering type material was deposited when the H_2S/ Zn molar input ratio is maintained at 0.5 or less. Depositions made under these process conditions, however, create numerous operational problems. For example, a fairly large fraction of the zinc passed into the deposition zone is not actually utilized in the deposit. As it exhausts from the mandrel into the cooler sections of the furnace and exhaust lines it condenses and has a tendency to clog the exhaust lines. This problem in turn can lead to the premature termination of the deposition. Furthermore, unless precautions are taken the condensed zinc droplets and dust can fall back into the deposition zone and be incorporated into the deposit before it has time to re-evaporate.

As a consequence of the above problems, we initially addressed ourselves to redesigning the exhaust end of the furnace, and the exhaust lines. The exhaust section of the furnace was redesigned in a manner that allowed the zinc dust to collect in a container as far removed from the exhaust lines as possible. In addition, a large dust collector drum was welded into the exhaust lines immediately adjacent to the furnace so that any zinc

dust that was exhausted from the furnace would be collected without clogging the exhaust lines. The exhaust section of the furnace was maintained at the appropriate temperature by adding an auxiliary heater to that section of the furnace. Furthermore, the top of the mandrel was covered so that there was no direct line of site from the exhaust to the actual deposition zone. This eliminated the possibility of condensed zinc falling back into the deposition zone.

Prior to depositing any material with the reworked exhaust system the first of the eighteen (18) runs (ZnS-97) that were made on this program was deposited in the original system. It was deposited under a standard set of operating conditions. Other runs were compared to it to determine the degree of improvement attained. The operating conditions used for all the runs are summarized in Table I. At this point in the program it was decided that all subsequent runs would be made at a deposition temperature of 650° C. This decision was based on the fact that at this temperature the deposition rate was still adequate (~ 0.005 in. / hr) and the amount of scatter observed was less than that observed at 700° and 750° C. An alternate to the above choice would have been to deposit material at 550° to 600° C. In this temperature range, however, the deposition rate is lower (~ 0.002 to 0.003 in. / hr), the material is browner in color and the 6 μm absorption band is deeper. Furthermore, it would have been necessary to maintain the retort temperature close to the temperature of the mandrel to obtain the desired zinc usage rate. This fact would have caused additional operational problems since the possibility of condensing zinc as it entered the deposition zone is increased due to the presence of the cooler hydrogen sulfide and carrier gas used with the H_2S. On the other hand, the imaging quality of the low temperature deposits is quite good and in retrospect depositions at these lower deposition temperatures should have been explored further.

The aforementioned changes made in the exhaust end of the furnace were modified several times to improve their performance. By the end of the program several 100-hour runs had been made without experiencing any operational problems. Process runs specifically concerned with the

TABLE I

ZINC SULFIDE DEPOSITION RUNS

Run No.	Mandrel Temp. (° C)	Retort Temp. (° C)	Furnace Pressure (torr)	H_2S Flow Rate (lpm)	Zn Usage (gm/hr)	Deposition Time (hrs)
ZnS-97	650	640	40	2.0	567	100
ZnS-98	650	600	40	2.0	300	10
ZnS-99	650	625	40	2.0	100	43
ZnS-100	650	620	40	2.0	300	45
ZnS-101	650	620	40	2.0	---	2
ZnS-102	725	650	40	1.0	230	10
ZnS-103	650	620	40	2.0	1100	33
ZnS-104	600	600	40	2.0	200	59
ZnS-105	625	610	40	2.0	1071	72
ZnS-106	650	615	40	2.0	817	110
ZnS-107	650	615	40	2.0	794	80
ZnS-108	650	630	40	2.0	820	100
ZnS-109	650	630	40	2.0	~800	12
ZnS-110	650	630	40	2.0	700	81
ZnS-111	650	610	40	2.0	980	100
ZnS-112	650	625	40	2.0	1000	60
ZnS-113	650	600	40	2.0	---	34
ZnS-114	650	650	40	2.0	900	105

evaluation of the exhaust system and the auxiliary heater were runs ZnS-101 and -103. These runs, as well as subsequent runs, indicated that the visible-to-the-eye zinc inclusion had been eliminated from the deposits. With the solution of this problem one of the objectives of the program was met.

At the same time that we were primarily attempting to eliminate large zinc inclusions and attempting to modify the equipment so that runs could operate to completion without major adjustments in process parameters, experiments were being performed on how best to supply a constant amount of zinc vapor throughout the run in order to eliminate or reduce bands in the material. In our previous process runs we had passed the carrier gas over the molten zinc and subsequently passed it into the deposition chamber. It was felt that if the carrier gas was bubbled through the zinc melt that the amount of zinc used per unit of time would be more uniform. A retort capable of handling this technique was designed and utilized initially in run ZnS-98. In run ZnS-99, which was of 43 hours duration, good imaging quality material was obtained without the presence of any pronounced banding. Subsequent runs of longer duration (for example, ZnS-106 and -107) indicated, however, that the problem had not been eliminated since bands of varying intensity were observed when the material was polished perpendicular to the deposition plane.

In an attempt to improve the homogeneity of the material, further improvements in the zinc retort were attempted. In run ZnS-109, for example, all the lines leading to the zinc retort were threaded in place. After 11 hours of deposition it was noted that the bubbling action had ceased and the run was terminated. When the retort was disassembled it was noted that some of the seals had loosened. Thus some of the argon gas had escaped without bubbling through the melt and as a result the zinc usage rate was not constant as a function of time. It is felt that this fact probably accounts for many of the bands observed in the process runs made with this type of retort design.

In view of these results the zinc retort was again redesigned so that

the majority of the carrier gas was passed over the surface of the melt with only a small amount of bubbling through the melt. The purpose of the gas bubbling through the melt was to keep the surface of the zinc melt agitated to prevent a scum layer from forming a coherent surface. (A coherent surface could cause a nonuniform zinc usage rate.) The scum layer is probably zinc oxide that floats to the surface when metallic zinc pellets are melted. The oxide layer is formed on zinc of even 99.999 percent purity. This retort design also incorporated a float mechanism that enabled us to measure the usage rate of zinc as a function of time. With the use of the float it was also possible to adjust the usage rate early in a run to attain the desired value. Even with this type of control of zinc usage rate, however, it was not possible to completely eliminate bands in the material. Evaluation of zinc usage versus time curves indicates the slope of the line for finite periods of time can vary significantly. If bands are formed by a nonuniform zinc usage rate it can be easily visualized why the bands are randomly dispersed in the material.

Figure 1 presents a typical in-line transmission curve (0.5 μm to 14 μm) for CVD zinc sulfide taken from one of the large plate runs. Two regions of the spectra are of particular interest if this material is to be used for multispectral window applications. The first region is between 0.5 and 1 μm and, as noted, the transmission gradually increases as the wavelength is increased. If the material were scatter-free and free of impurities it would rise exponentially at the absorption edge and exhibit approximately 68 percent transmission until multiphonon region was approached. The major cause for the observed difference is probably scatter, although there is obviously some type of impurity absorption, particularly near the absorption edge. Figure 2 shows the transmission of essentially colorless ZnS and, as noted, there is a much sharper absorption edge. Between ~0.45 and 2 μm, however, the shape of the curve indicates that the material still has scatter sites.

The second region of interest for multispectral window applications is between 8 and 11.5 μm. In this region CVD ZnS performs satisfactorily until ~10 μm. Beyond this wavelength multiphonon absorptions are in

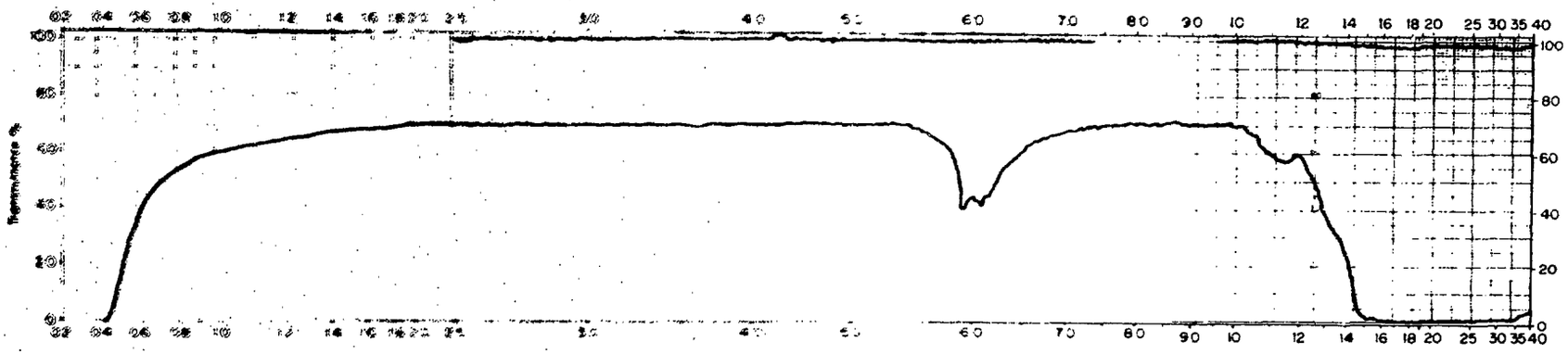

Fig. 1 Typical In-Line Transmission Curve (0.5 to 14 μm) for CVD ZnS taken from a Large Plate Run, t = 0.202 in.

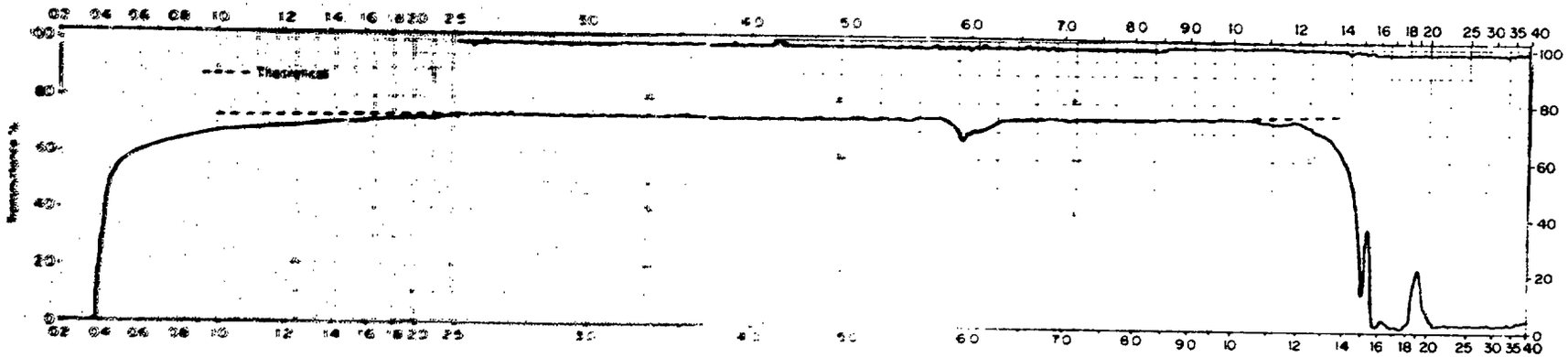

Fig. 2 In-Line Transmission of Essentially Colorless ZnS
Thickness = 0.035 in.

evidence and the percent transmission is decreased. If the material is to transmit to ~11.5 μm it must be made stronger so that thinner cross-sections can be used, or alternatively, the composition of the zinc sulfide should be altered. The latter approach to the problem was investigated under Contract No. F33615-72-C-1501, and Fig. 3 shows a typical transmission curve for a zinc selenide-sulfide solid solution. As noted, good transmission is obtained to ~13 μm. At the visible end of the spectrum the material still exhibits some scatter and absorption, and further work is needed to deposit an optimum material.

There is no fundamental reason why CVD zinc sulfide cannot be made scatter-free and colorless. To accomplish this, however, a better understanding of the cause of scattering is needed. In our opinion, scattering is due to microporosity. Microporosity is caused by either/or the formation and decomposition of zinc hydride during deposition or by the formation of small amounts of hexagonal zinc sulfide along with the cubic phase. Techniques are currently being investigated to suppress the formation of zinc hydride under Contract No. F33615-72-C-1501. Appropriate dopants could be added to suppress the formation of the hexagonal phase of zinc sulfide.

As experiments were being made to improve the homogeneity of the material, the mandrel design was also being altered to eliminate cracking of the deposit. Deposited plates fracture when they are not free to contract during cooldown from the deposition temperature. Numerous designs were tried to isolate the deposit from the other furnace components within the furnace that become coated with ZnS. A design that appears to have solved the problem utilized tantalum metal as a mandrel terminator. Use of this material resulted in essentially crack-free plates following run ZnS-108. With the solution of this problem a second objective of the program was met.

Improvement of the thickness profile of large plates (14 × 20 in.) was the final problem investigated. Several factors appear to govern the type of thickness profile attained. The more important of these factors are:

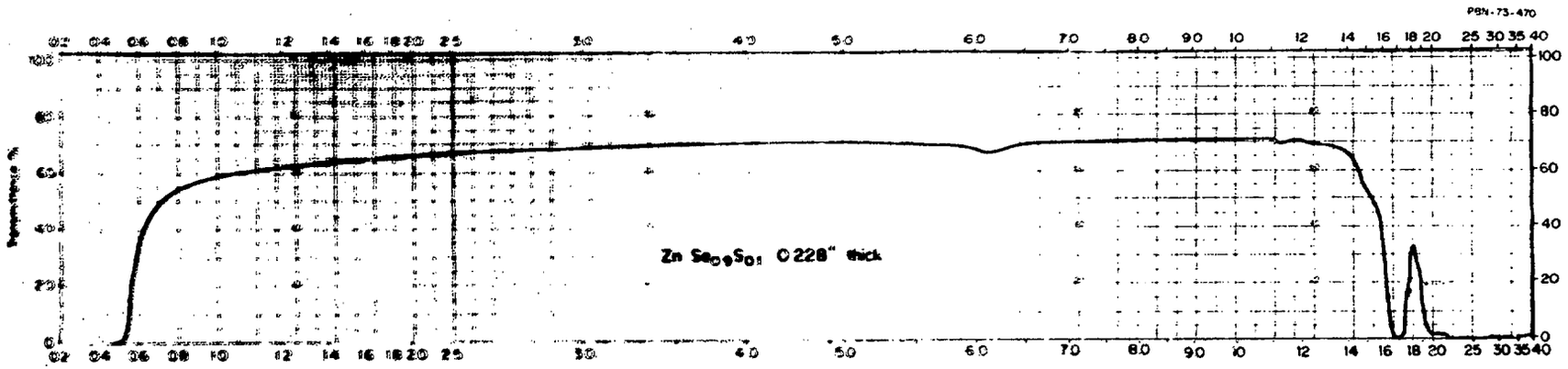

Fig. 3 Typical In-Line Transmission Curve (0.5 to 22 μm) for CVD Zinc-Sulfo-Selenide Solid Solution Taken from a 2 X 4 in. plate.

1) Flow pattern of the reactants
2) Velocity of the reactants
3) Degree of premixing and temperature of the reactants prior to their entrance into the mandrel.

Several runs (for example, ZnS-103, -104, -108) were primarily concerned with attempts to improve the thickness profile by altering the flow pattern and velocity of the reactants. Other process runs, ZnS-110 for example, evaluated the effect of premixing of the reactants. Analysis of profile from these runs indicated that there was no single factor that controlled the thickness distribution, but rather that a balance had to be maintained between premixing and velocity. Figures 4 and 5 illustrate the differences in thickness distribution that were attained. In the case of the profile shown in Fig. 4, a significant amount of premixing of the reactants was allowed and as a result the material is deposited as soon as it enters the mandrel. By separating the zinc vapor and H_2S gas until they enter the mandrel, the heavy deposit at the entrance of the mandrel can be prevented and a more uniform profile can be attained (Fig. 5). In this latter run the velocity of the H_2S gas was also lowered to allow more heating of the gas prior to its entrance into the mandrel. Repeated attainment of the above thickness profile would significantly lower the cost of FLIR-type windows.

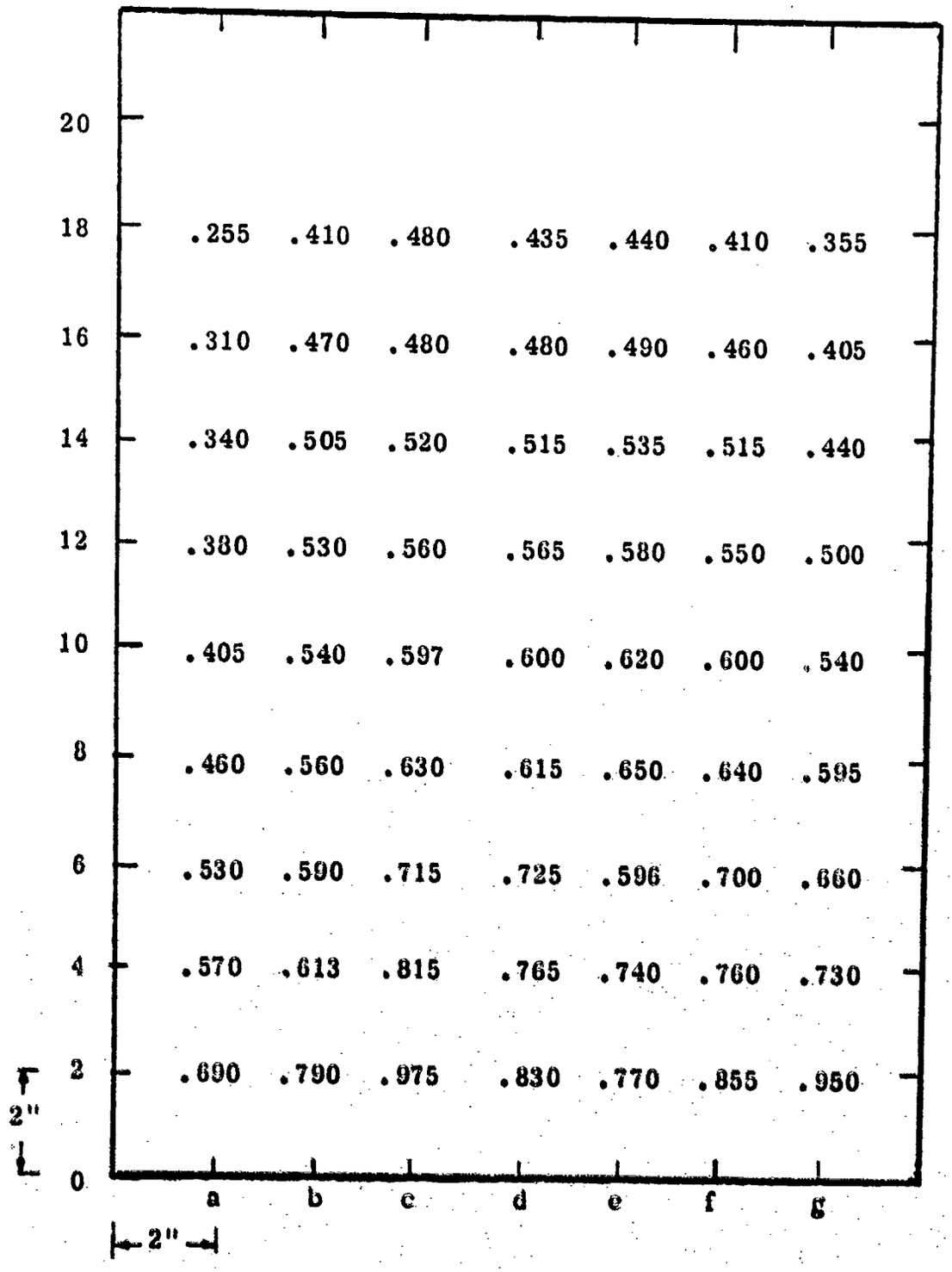

Fig. 4 Deposition Profile - Run ZnS-96, Plate A

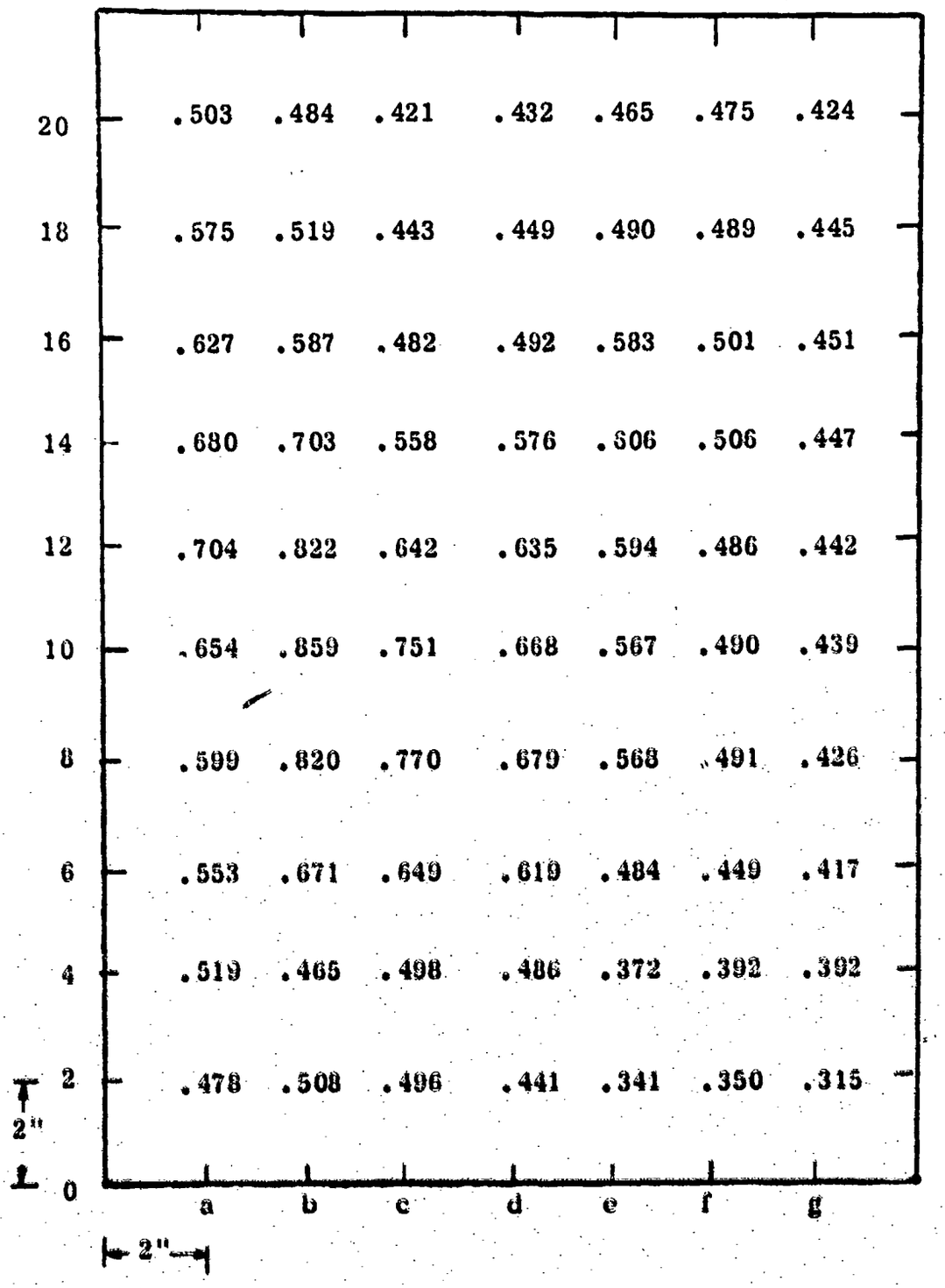

Fig. 5 Deposition Profile - Run ZnS-111, Plate A

SECTION IV
OPTICAL CHARACTERIZATION OF CVD ZINC SULFIDE

Potential applications for CVD ZnS material include aircraft windows and domes for use in four wavelength ranges. These are the long wavelength infrared 8-13 μm band, used primarily for passive infrared sensing of objects at temperatures near 300° K, the mid infrared 3-5 μm for hot body tracking, the range 0.8 to 1.06 μm for active laser systems, and the visible-near-infrared 0.4 to 0.9 μm range for low light level TV systems. Stoichiometric, scatter-free zinc sulfide should be transparent to all wavelengths between 0.4 and 10.5 μm, limited at each end by intrinsic electronic and multiphonon bands respectively, and can be used in principle in all four ranges. In practice, the long wavelength limit is indeed set by intrinsic absorption bands, but extrinsic processes can reduce transparency at shorter wavelengths. Thus the CVD material shows an extrinsic band near 6 μm that we attribute to a ZnH_2 vibrational absorption, a broadband absorption in the visible region associated with excess zinc in the lattice, and a scattering component extending from 2 μm to shorter wavelengths that is probably due to residual microporosity in the range of 100 ppm.

The overall reduction in signal intensity in a typical scene covering a 5° × 5° field of view is well represented by the scanning spectrometer traces of Figs. 1 - 3. These traces are affected by radiation absorbed directly in the test plate, and by radiation scattered at angles larger than the acceptance angle of the spectrometer, usually a few degrees. Beyond this measure, it is necessary to characterize the effect on image quality of transmission through a typical sample thickness. This effect is governed by scattering from particulate matter, voids, or surface scratches on the one hand, and on the other by any variation of optical path due to density changes, stress or polarization effects.

The CVD zinc sulfide material shows first, a widespread distribution of microscopic pores and in some cases, of zinc particles that dominate

the large angle scatter at short wavelengths and contribute most of the scatter at angles less than 5°. The prime effect of this type of defect will be a general increase in background and lowering of image contrast - it will have no significant effect on geometric image resolution. Furthermore, in a typical infrared imaging system designed to distinguish small emissivity or temperature changes in a scene near 300° K, that is to say in a scene where the contrast is already very low, the net effect of scatter on image contrast will be very small.

Second, using polarized light a small scale structure can be seen in CVD chalcogenides that is related to the growth habit. Optical path length changes of the order of $\lambda / 2$ peak-to-peak in the visible appear in random patterns with a typical spatial scale of approximately 1 mm. This type of perturbation will produce diffuse halos around images at angles of deviation of the order of 1 mrad at visible wavelengths, and 10 mrads at 10 μm wavelengths. Again, in an optical system with a typical aperture of 10 - 20 cm these perturbations could be considered to effect image contrast more than the image sharpness.

Finally, there are potential variations of refractive index on scales comparable with the deposition chamber itself, and therefore comparable with the optical apertues of typical windows and lens components. In principle these variations will affect the resolution of fine-scale image structure and will appear either as a geometric distortion or as an image spread depending on the spatial variations of refractive index in a particular plate.

Two attempts have been made to characterize these image perturbation effects by interferometric measurements on test plates using laser sources either at 0.6328 μm in the visible, or at 10.6 μm in the infrared. In these, surface interferograms at 0.6328 μm were taken of each face separately, followed by an interferogram in a double pass interferometer. This data was then analyzed to give a map of optical path length over the plate, and to separate out the contribution to that path change due to variations of index internal to the plate.

The first set of measurements, taken at Itek Corp., were made on a 1 in. dia. sample, 3 mm thick. In this case, all tests were performed with a Twyman-Green interferometer using a wavelength of 0.6328 μm. Six interferograms were used in the analysis. The first pair of two, one with horizontal and one with vertical fringes, was of the wavefront reflected from side 1 of the test piece. The second pair of two interferograms was of the wavefront reflected from side 2. Finally, two interferograms of the double-pass transmitted wavefront through the test piece were used; side 1 was facing the interferometer. The interferograms are shown in Figs. 6, 7 and 8. The errors in the interferometer, including the beam expander, beam splitter and mirrors, was less than 0.05 λ peak-to-peak. This was obtained by inspection of the fringe pattern when the sample was not in place.

The object of the test was to determine the wavefront degradation and MTF degradation due to inhomogeneities in the material. Measurements of both surfaces, as well as transmission, were used to eliminate the effects of surface errors. The data from each interferogram was fitted with a 28 term Zernike polynomial and the results for the vertical and horizontal fringe orientations for each test were averaged to give the representation of the wavefront. Contour maps of these wavefronts are shown in Figs. 9, 10 and 11. The sign convention used is that wavefronts which are convex as they return to the interferometer are negative at the center.

In order to find the transmitted wavefront in the absence of surface errors, the following relationship was used:

$$W_4 = W_3 + (N-1)(W_1 + W_2)$$

where: W_1 is the reflected wavefront from side 1
W_2 is the reflected wavefront from side 2
W_3 is the double-pass transmitted wavefront
W_4 is the double-pass transmitted wavefront in the absence of surface errors
N is the index of refraction of the material.

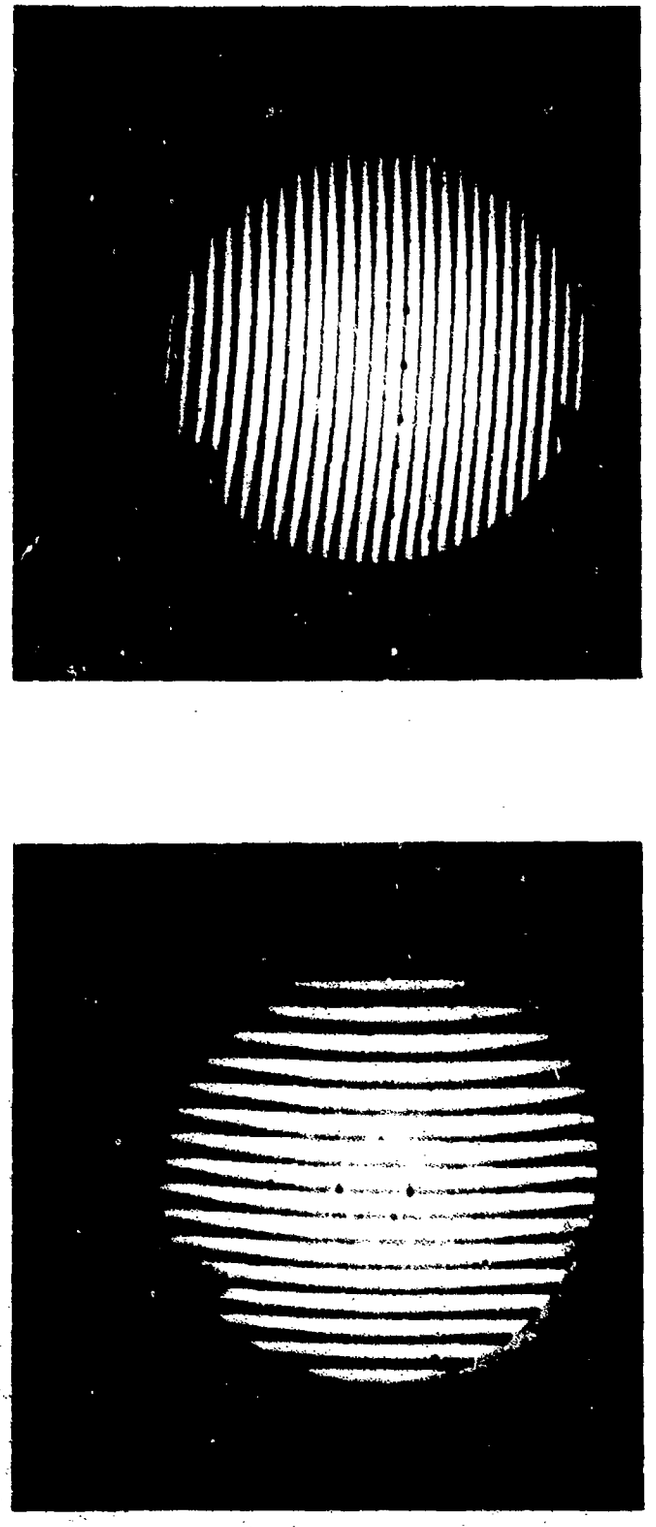

Fig. 6 Interferograms of Surface Reflection From Side 1

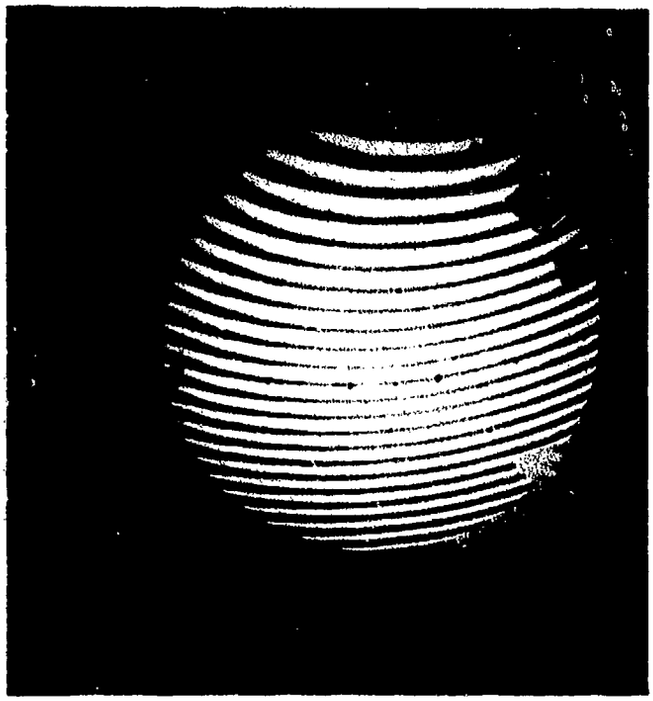

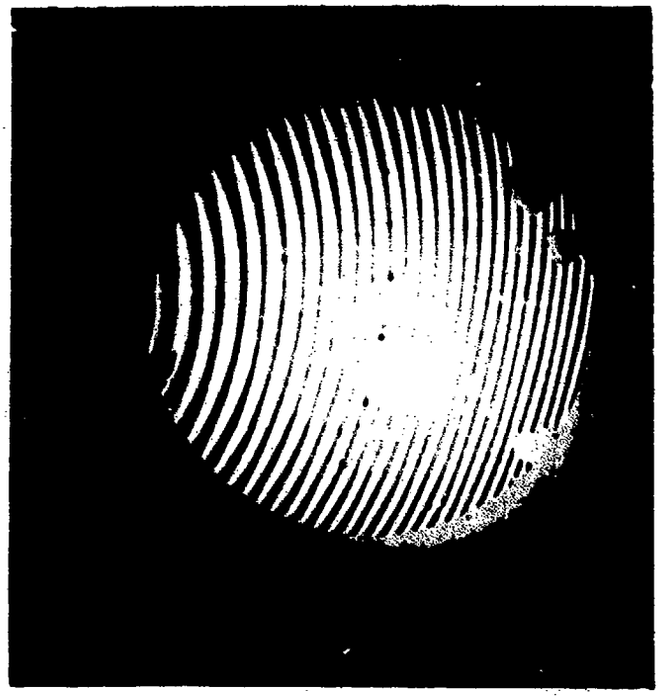

Fig. 7 **Interferograms of Surface Reflection From Side 2**

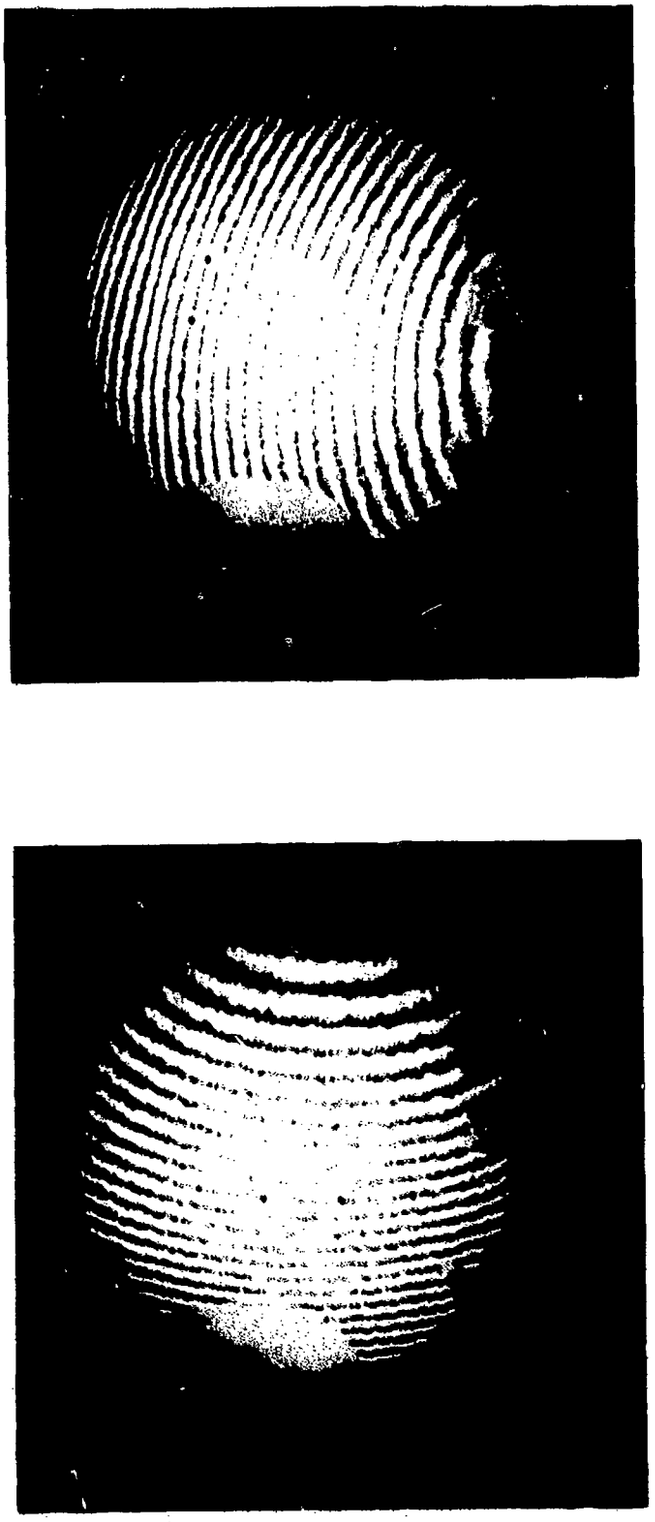

Fig. 8 Interferograms of Double-Pass Transmission

RMS = .20λ

PK - PK = .77λ

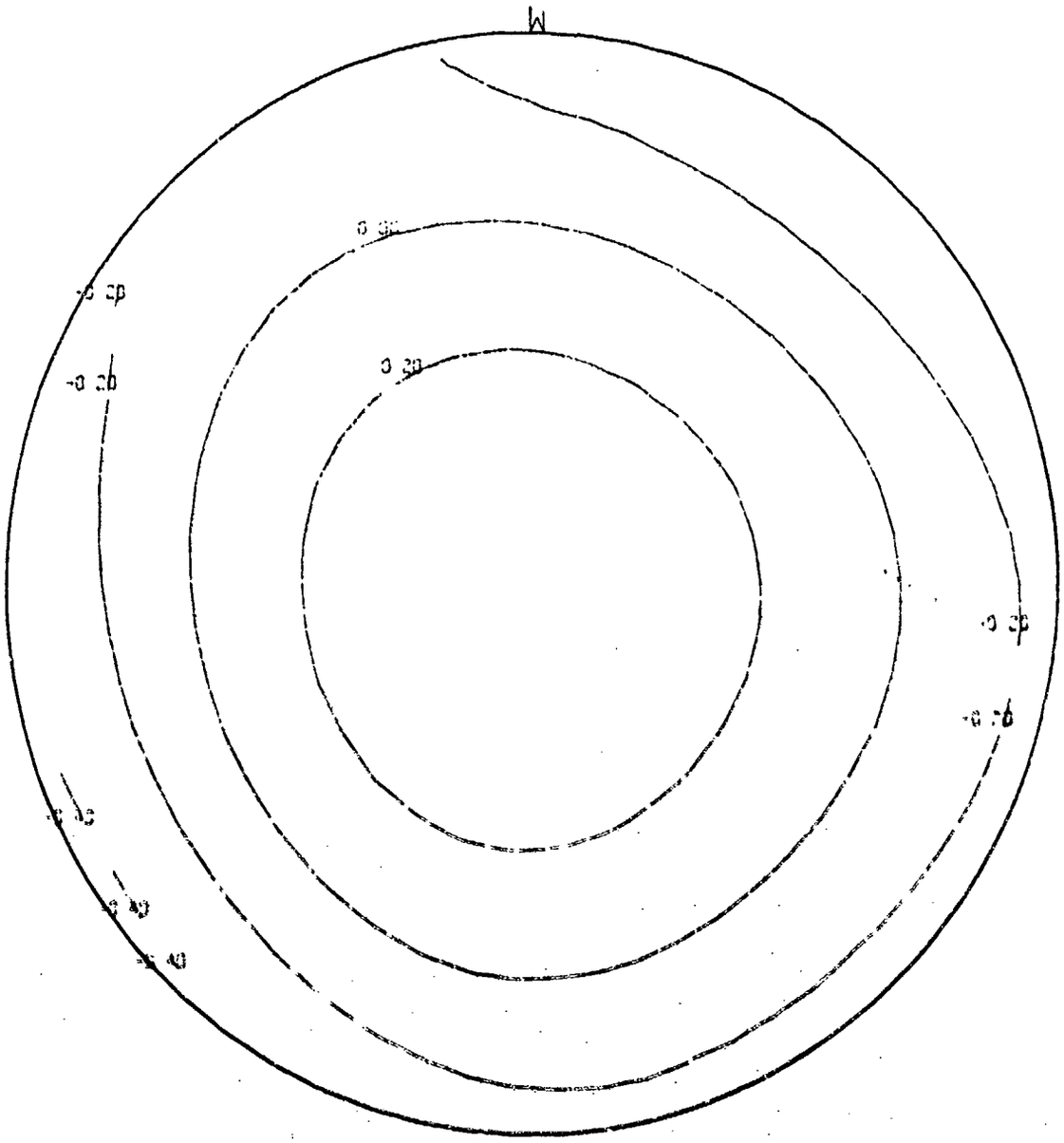

Fig. 9 **Reflected Wavefront From Side 1 of Test Piece**

RMS = 1.03λ

PK – PK = 4.57λ

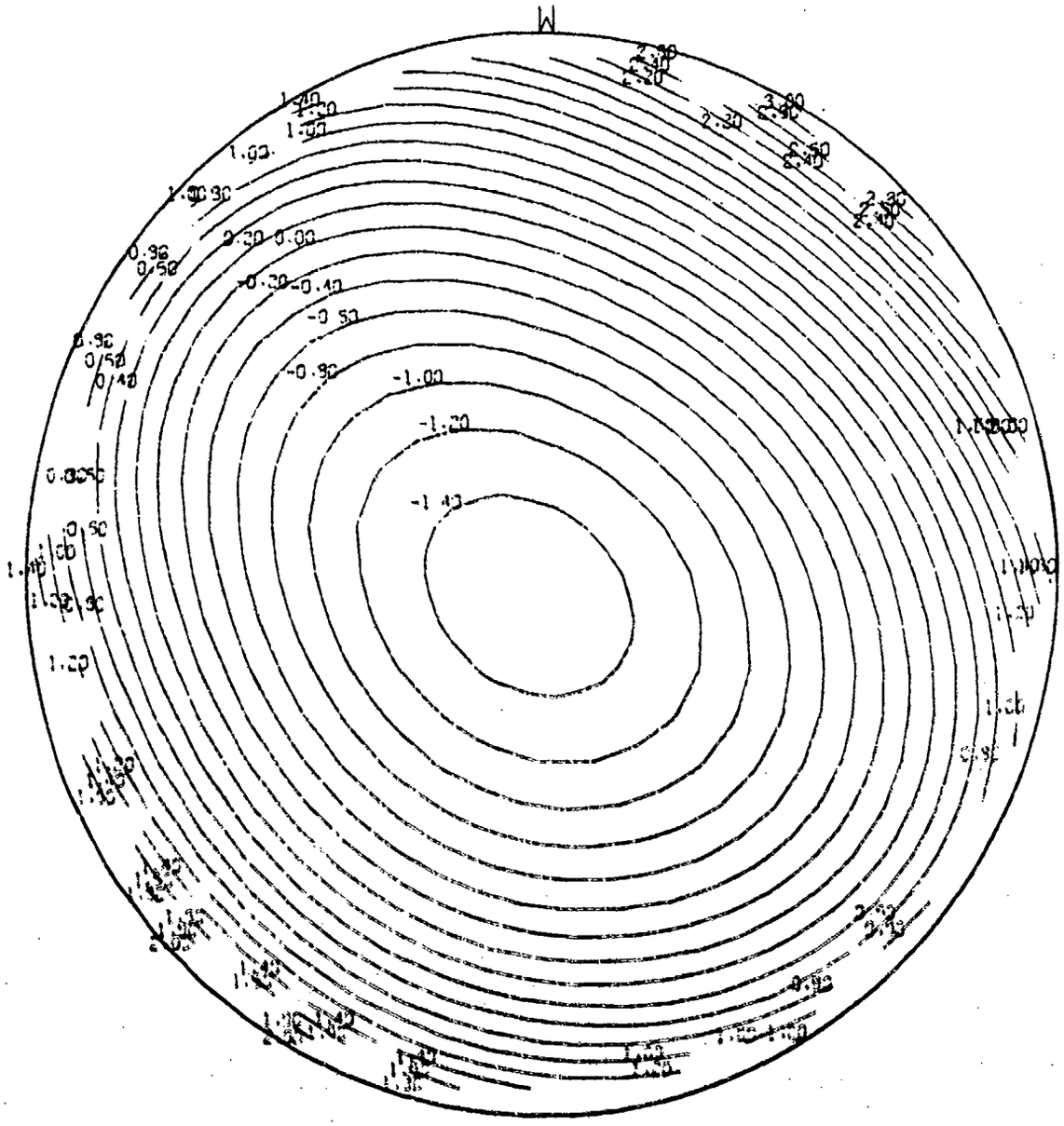

Fig. 10 **Reflected Wavefront From Side 2 of Test Piece**

RMS = 1.13λ

PK - PK = 4.98λ

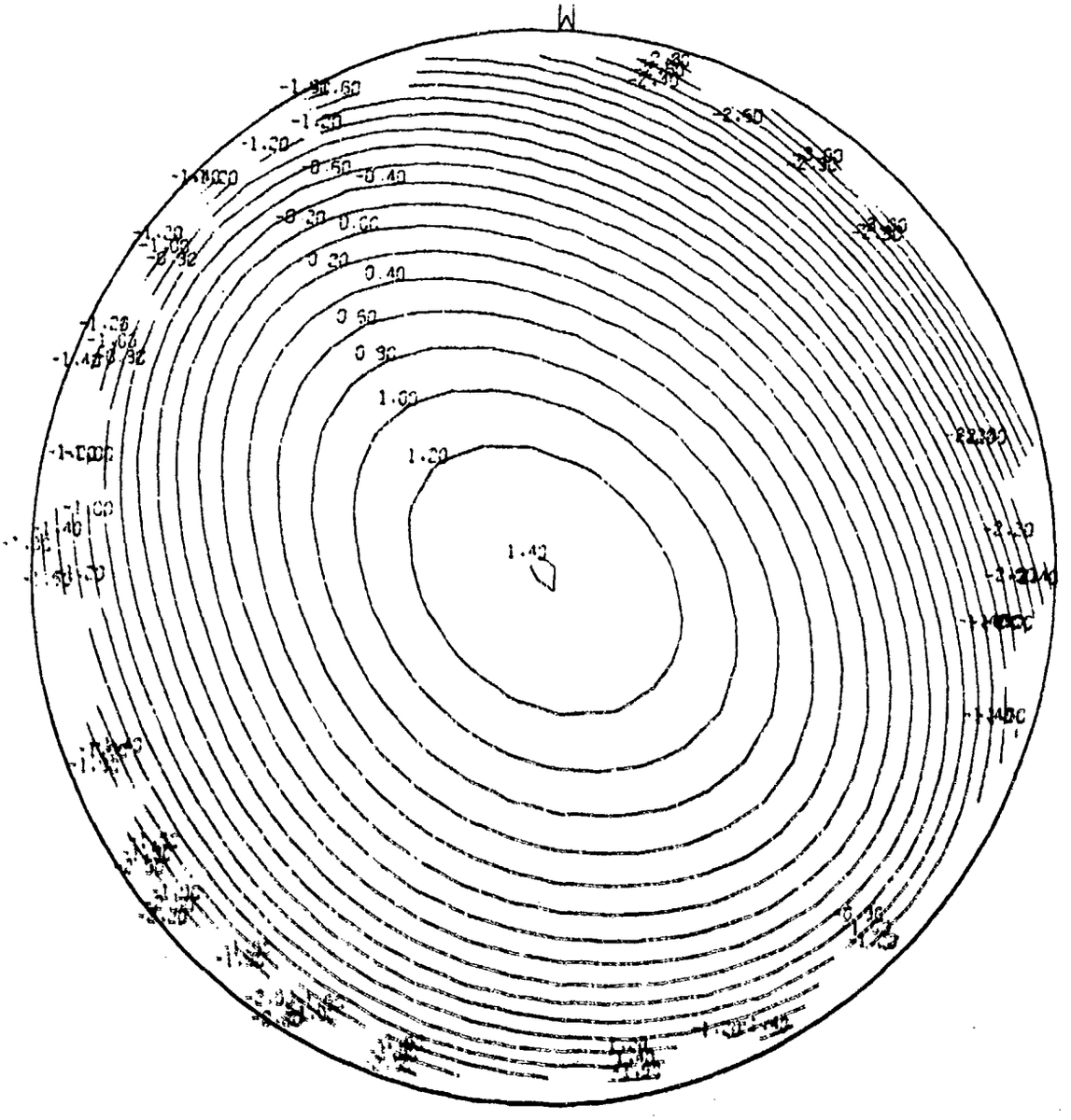

Fig. 11 Double-Pass Transmitted Wavefront Through Test Piece

A value of N = 2.35 was used.* The error in this number is estimated to be 0.01. A contour map of W_4 is shown in Fig. 12.

The nature of the inhomogeneities in the material was found to be of two types. The first was a gross variation over the 1-inch diameter which was very smooth. It appears to have frequency components larger than 1 cycle/inch. The magnitude of this variation in single-pass was determined to be 0.37λ peak-to-peak, 0.075λ RMS. The uncertainty in this result due to lack of precise index of refraction data is about 0.005λ RMS. However, additional uncertainty due to data reduction limitations is estimated to be as large as .10λ RMS. When carrying out the analysis described in the previous section, the interferograms must be aligned precisely. Errors in the alignment result in large anomalies because of the steep slopes in the surface errors of side 2. Thus, the gross variation cannot definitely be attributed to index variation and samples with much better surfaces will have to be measured before this variation can be determined.

The second type of inhomogeneity is high frequency ripple. To measure the effects of this, two central fringes from an interferogram of the transmitted wavefront were scanned at very small intervals along their length. The frequency components of this variation appear to be much less than 10 cycles/inch. The magnitude of the disturbance in single-pass was 0.04 waves RMS at 0.6328 μm.

A good measure of optical quality is the RMS wavefront error given in units of wavelength. An RMS of .05 waves (at any wavelength) is considered diffraction limited. The total RMS wavefront degradation for the measured material is 0.04 waves at 0.6328 μm, assuming no gross variation in index of refraction. This number will scale inversely with wavelength

---

*Kodak Publication U-72, Herzberger Dispersion Formula for Irtran-2, extrapolation of 1-10 μm index data, pp. 13-14.

RMS = .15λ

PK - PK = .74λ

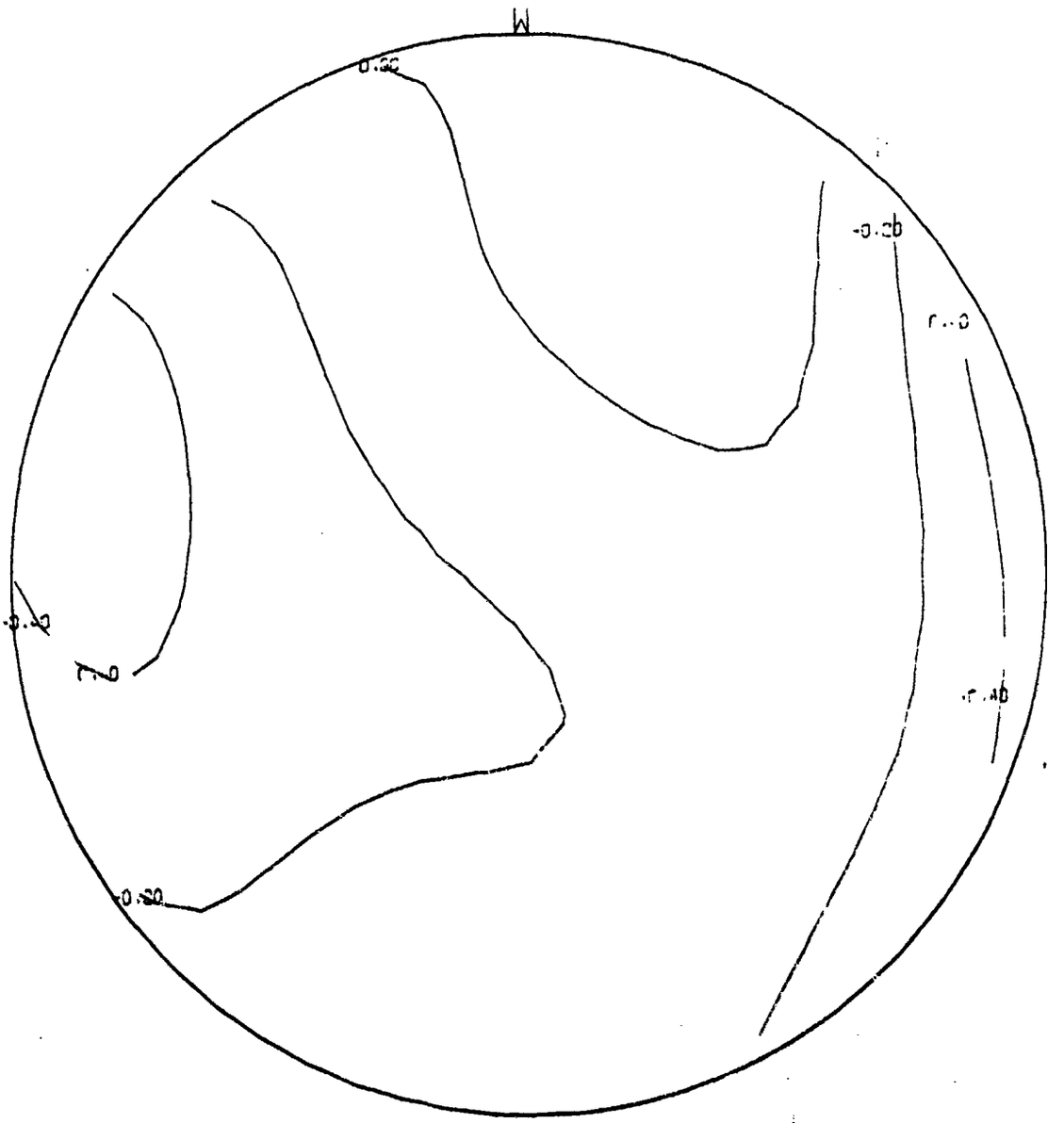

Fig. 12 Double-Pass Wavefront Error Due to Transmission in the Absence of Surface Errors

for other wavelengths. The variation with thickness is not as well defined; however, in general, the wavefront degradation will increase with increasing thickness.

For random wavefront errors, the MTF degradation is given by*

$$M = e^{-(2\pi\sigma)^2 (1-\theta)}$$

where σ is the RMS wavefront error and θ is the autocorrelation function of the wavefront error. For the high frequency variations noted in the sample, θ is essentially zero for all spatial frequencies of interest. The MTF degradation is then

$$M = e^{-[2\pi (.04)]^2} = 0.94 \text{ (at } 0.6328 \ \mu\text{m wavelength)}$$

Thus, the MTF of a system using this sample as a window will be 94 percent of the MTF without the window. For longer wavelengths, the degradation will be less.

A second set of interferometer measurements and analysis, carried out at Perkin Elmer Corp., were made on a 9 in. dia window, 0.4 in. in thickness. Their report is reproduced in part as follows.

1.0 OPTICAL PROCESSING

Upon receipt of the raw material, all pieces were ground on both sides to remove the outer "skin" and given a cloth polish. The pieces were inspected and the depth of the heavy striation in relation to the surface was measured. In order to remove this striation, it was necessary to grind 0.060 in. from the face of the window. This surface was given an optical

---

*E. L. O'Neill, Introduction to Statistical Optics (Addison-Wesley, 1963), p. 99.

polish with a surface figures of 1 wave.* The second surface was optically polished flat to within about 2 waves. For best accuracy in analysis, it is desirable to adjust the wedge angle between front and rear window surfaces in order to obtain between 15 and 20 fringes across the clear aperture when observing internal interference fringes. Up until this point, the wedge had been mechanically controlled. In order to optimize the wedge angle, an internal Fizeau interferogram was required. However, as described in a later section, this was not easily accomplished.

After testing the window was returned to the polishing shop for polishing to the final surface specifications. Some difficulty was experienced due to self weight deflection caused by the high diameter/thickness ratio and to changes in thermal environment between the polishing shop and the metrology laboratory.

2.0 OPTICAL TESTING

a. Surface Flatness

Figures 13 and 14 show interferograms taken of the surface on the finished 9-inch dia. window. These were recorded with the window mounted on edge. The reference surface was an uncoated fused silica flat placed in close proximity to, but not touching, the test window. The first surface is very flat. It is high at the center and edge with respect to the 0.7 radius zone. It is slightly convex. The best fit convex spherical surface is 0.12λ over the clear aperture. The second surface is concave and slight cylindrical in shape. The best fit sphere is concave by 0.37λ over the clear aperture. The two surfaces are matched to within $\lambda / 4$ as required. They are each flat to within 1 wave as specified.

---

*Unless otherwise specified, all measurements may be assumed to have been made at a wavelength of 0.6328 μm.

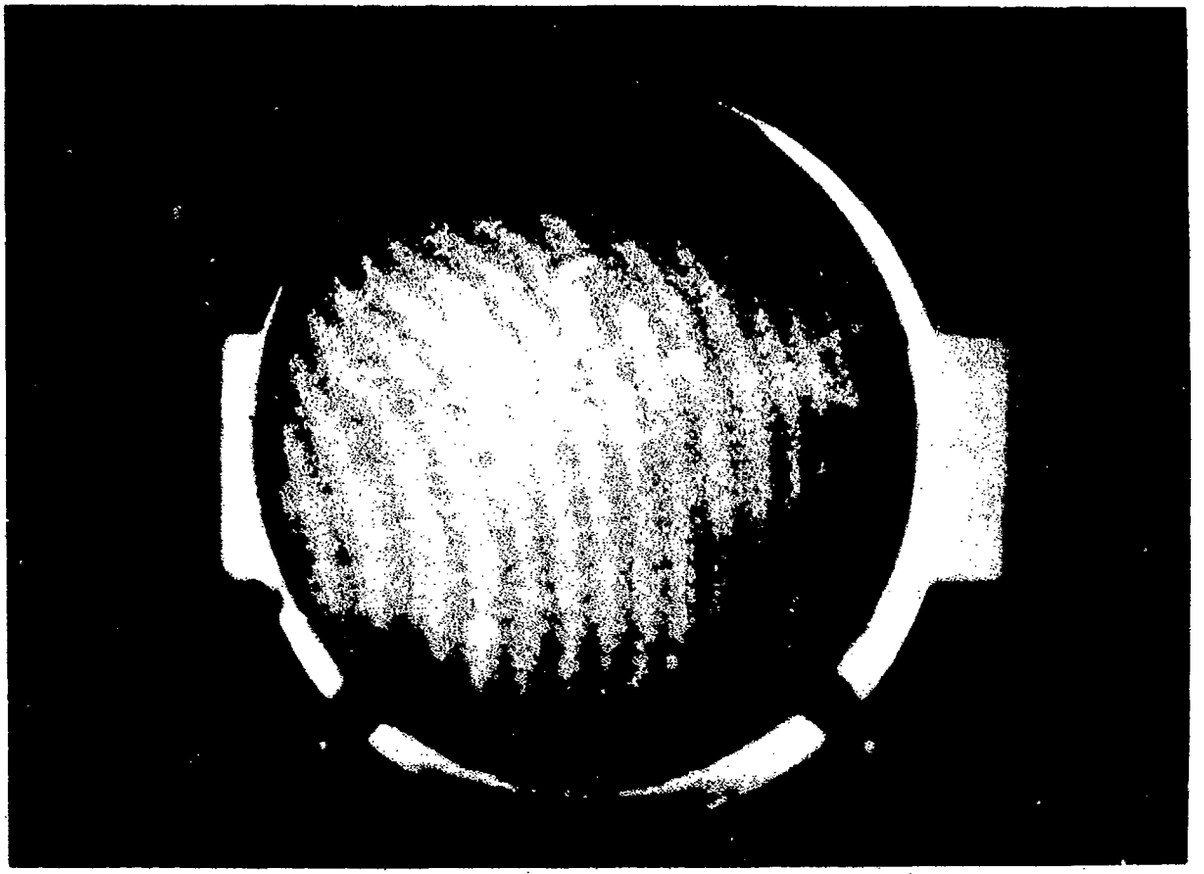

Fig. 13 Interferogram of First Window Surface

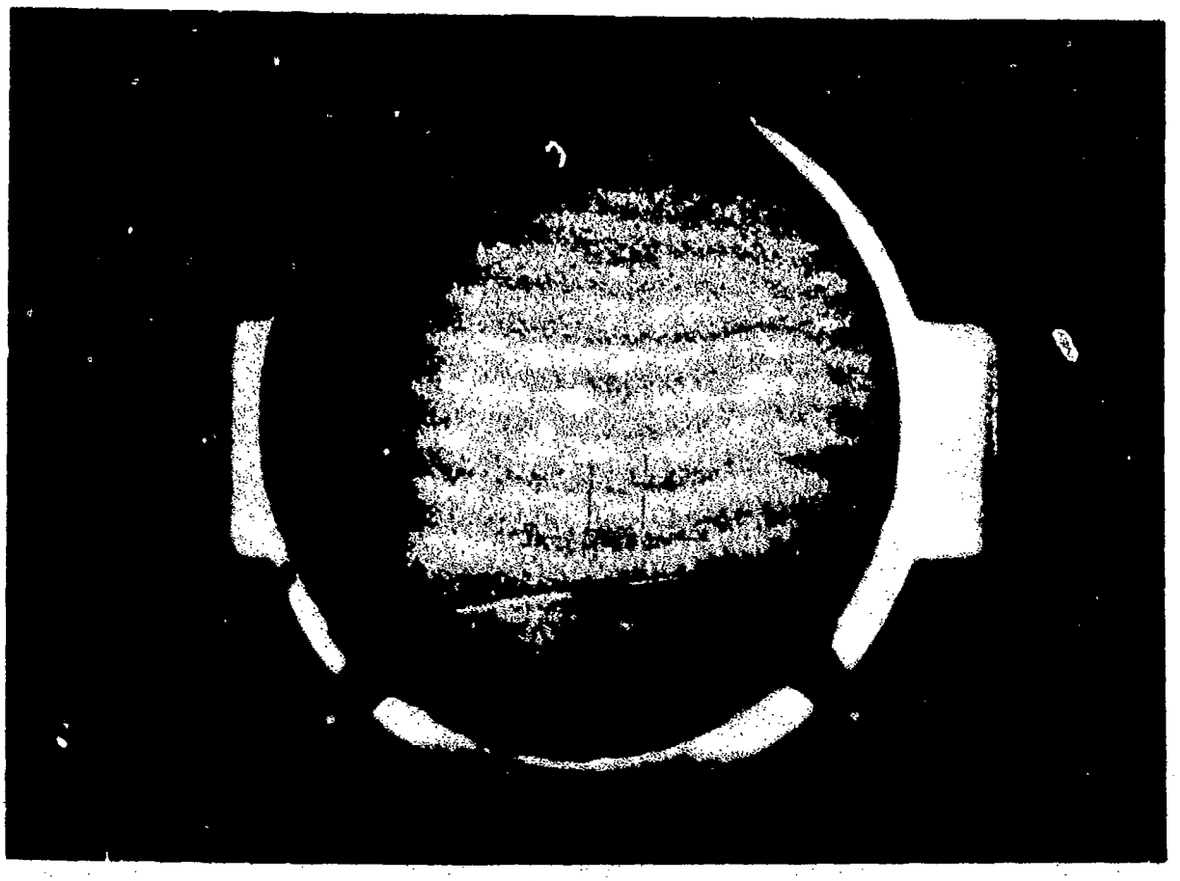

Fig. 14 Interferogram of Second Window Surface

b. Optical Homogeneity

The homogeneity of refractive index of a window must be determined interferometrically from two independent measurements. This is normally done by observing the window in transmission and by observing the internal Fizeau interference between reflections from the front and rear surfaces. However, due to the high level of internal scatter and absorption, no interference could be achieved. Transmission in single-pass was measured to be 7%. Since the interfering beam from the rear surface must pass through the window twice, the effective transmission is about 0.5%. Several special techniques were tried without success. These techniques included methods to maximize the fringe contrast by equalizing the amplitudes of both interfering beams. Failure to obtain an interferogram would have made index homogeneity measurements as well as MTF and PSF calculations impossible. The window was then placed in a 10.6 μm laser beam approximately 5 in. in dia. and internal Fizeau fringes were observed in transmission. The IR image was visually observed on a fluorescent image converter screen. While the fringes observed were of low contrast and difficult to photograph, they could readily be seen by eye. Based upon visual observations, the window appeared to have good homogeneity over its entire aperture. It was noted that some areas had visible defects. These areas showed variations in transmittance, but were not areas of differing index, since they did not distort the interference fringes. The estimated experimental sensitivity was $\pm 5 \times 10^{-5}$. A photograph of the fringe pattern was taken and computer-reduced. In combination with the surface interferograms this data was used to generate an index homogeneity map of the window center. Due to the poor quality of the infrared photos obtained, and the unknown degree of collimation in the illuminating beam, it is felt that the accuracy of the analytic determination is less than obtained from visual measurements of the IR fringes. Figure 15 shows the homogeneity map at 10.6 μm of the window center obtained from the raw data. Each contour represents a change of 1×10^{-4} in index. The contours are roughly circular and vary by about $\pm 1.5 \times 10^{-4}$ from nominal (contour NO). This apparent index "gradient" may be due, at least in part, to

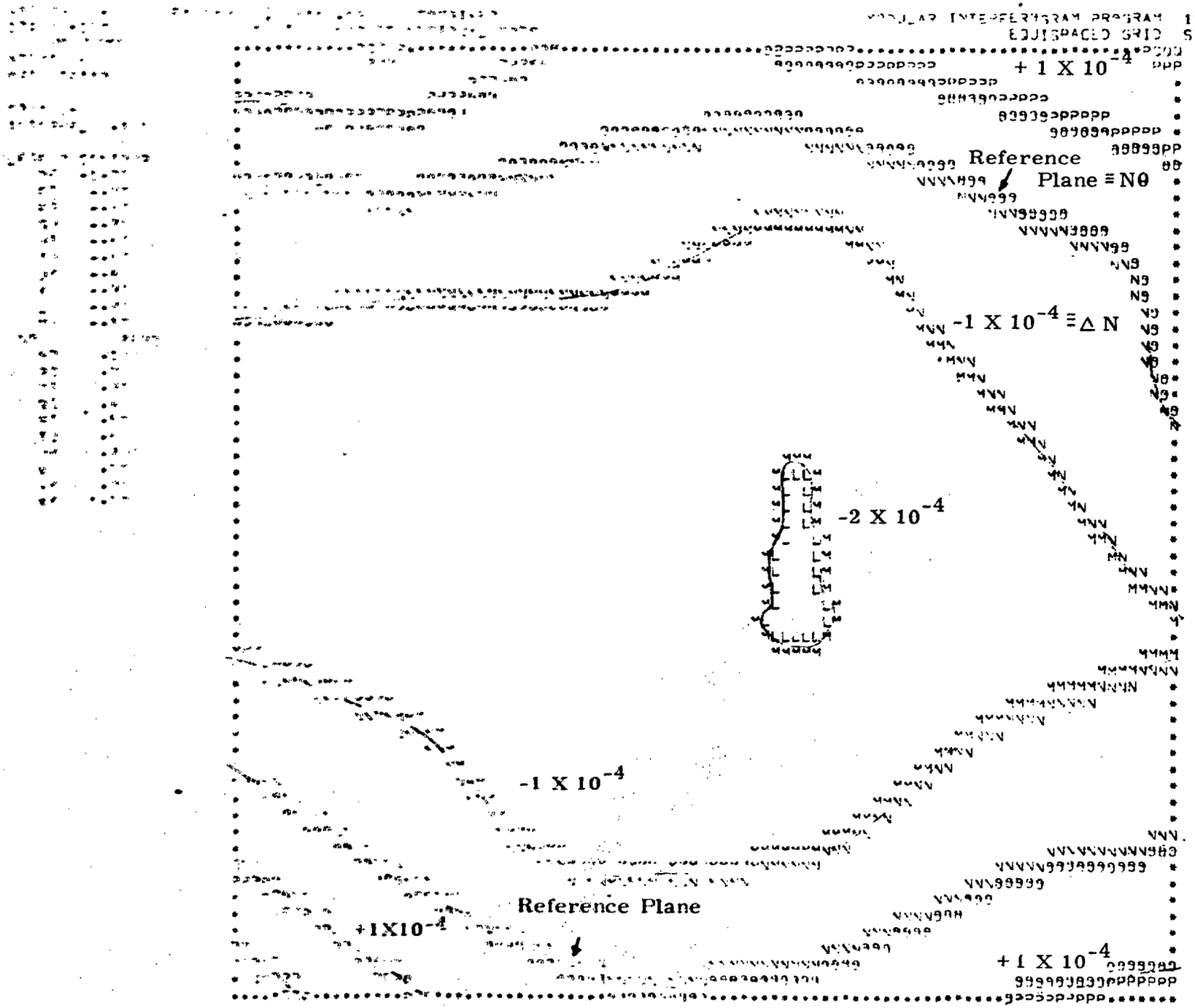

HOMOGENEITY MAP OF WINDOW AT 10.6μm
FIGURE 15

slightly divergent illuminating beam. If one removes all spherical terms from the data, the results are shown in Fig. 15A. Variations are less than $\pm 1 \times 10^{-4}$ in this case, which agrees well with visual observations.

Figures 16 and 16A show Optical Path Difference maps of the transmitted wavefront through the window for 0.9 μm and 10.6 μm generated from raw data. Figures 17 and 17A are the same, but with the spherical terms removed. This corresponds to the situation in which the illuminating optical transmitter is re-focussed to minimize the effects of the radially symmetric window inhomogeneities (if indeed they are real) and any other optical "power" present in the window.

c. Calculation of MTF and PSF

Based upon the calculated Optical Path Differences over the central 3 in. of the window aperture both the tangential and saggital MTF's can be calculated. The results are shown in Figs. 18 through 22. Figure 18 shows a qualitative isometric view of the MTF for 10.6 μm, while Fig. 19 shows the same plot at best focus. These plots are very symmetric, regular, and are almost indistinguishable from each other. They all represent nearly diffraction limited performance. Figure 20 is a representative numerical plot of the MTF at 10.6 μm at best focus. The upper curve corresponds to the diffraction limited case.

Figure 21 is a qualitative view of the PSF at 10.6 μm, while Fig. 22 is at best focus. Figure 23 is a numerical plot of the PSF (for 10.6 μm) of the window "as is" and at best focus. If the volume under the curve is taken as unity, then for a diffraction limited system, the intensity on-axis should be 0.05. As is evident from the graph, the curve does peak for best focus at very nearly the diffraction limit. The distribution is slightly asymmetric about the optical axis for either case and is due to the slight residual non-symmetries of the transmitted OPD maps.

HOMOGENEITY MAP OF WINDOW AT 10.6μm
WITH POWER REMOVAL (AT BEST FOCUS)
FIGURE 15A

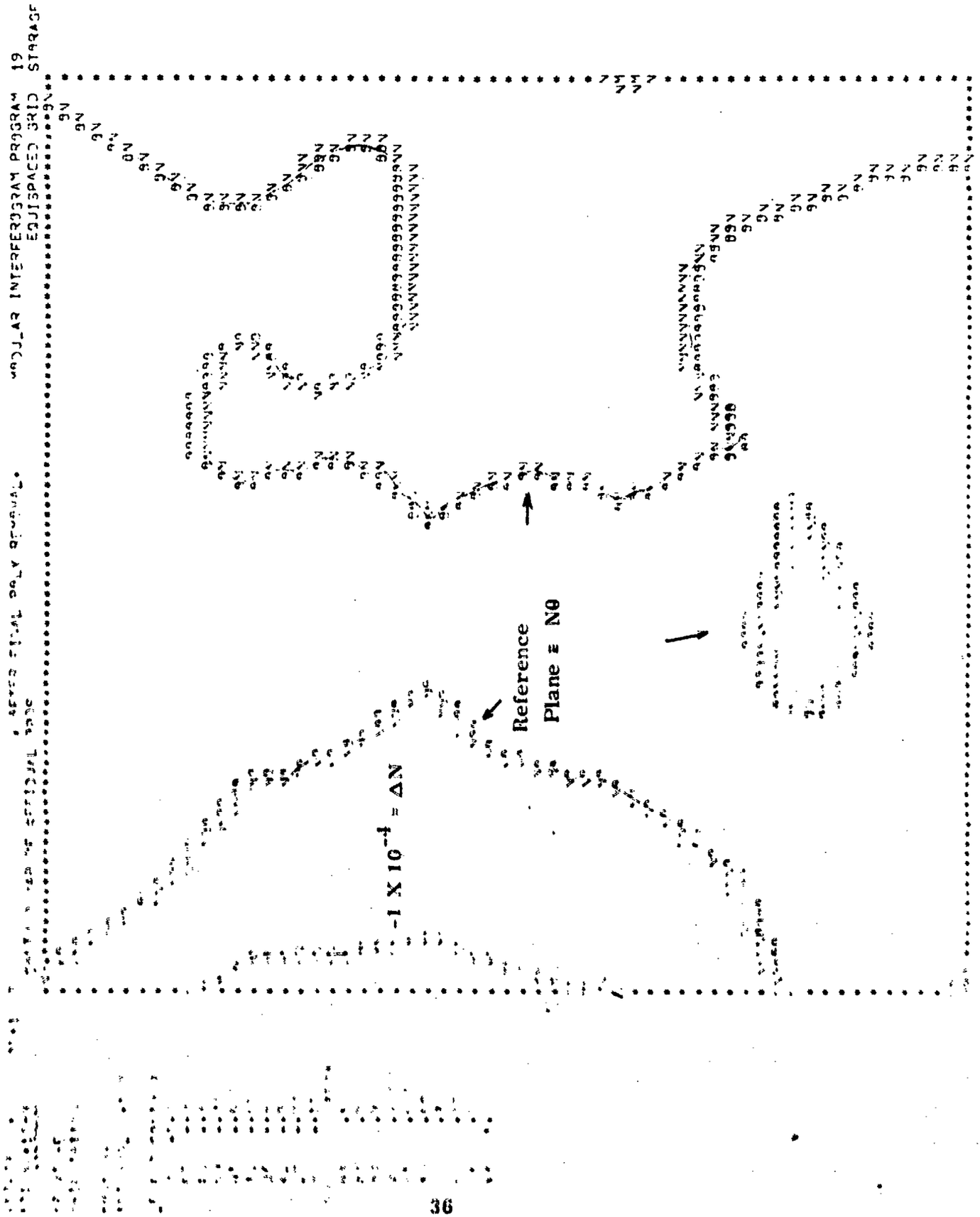

TRANSMITTED WAVEFRONT AT 0.9μm

FIGURE 16

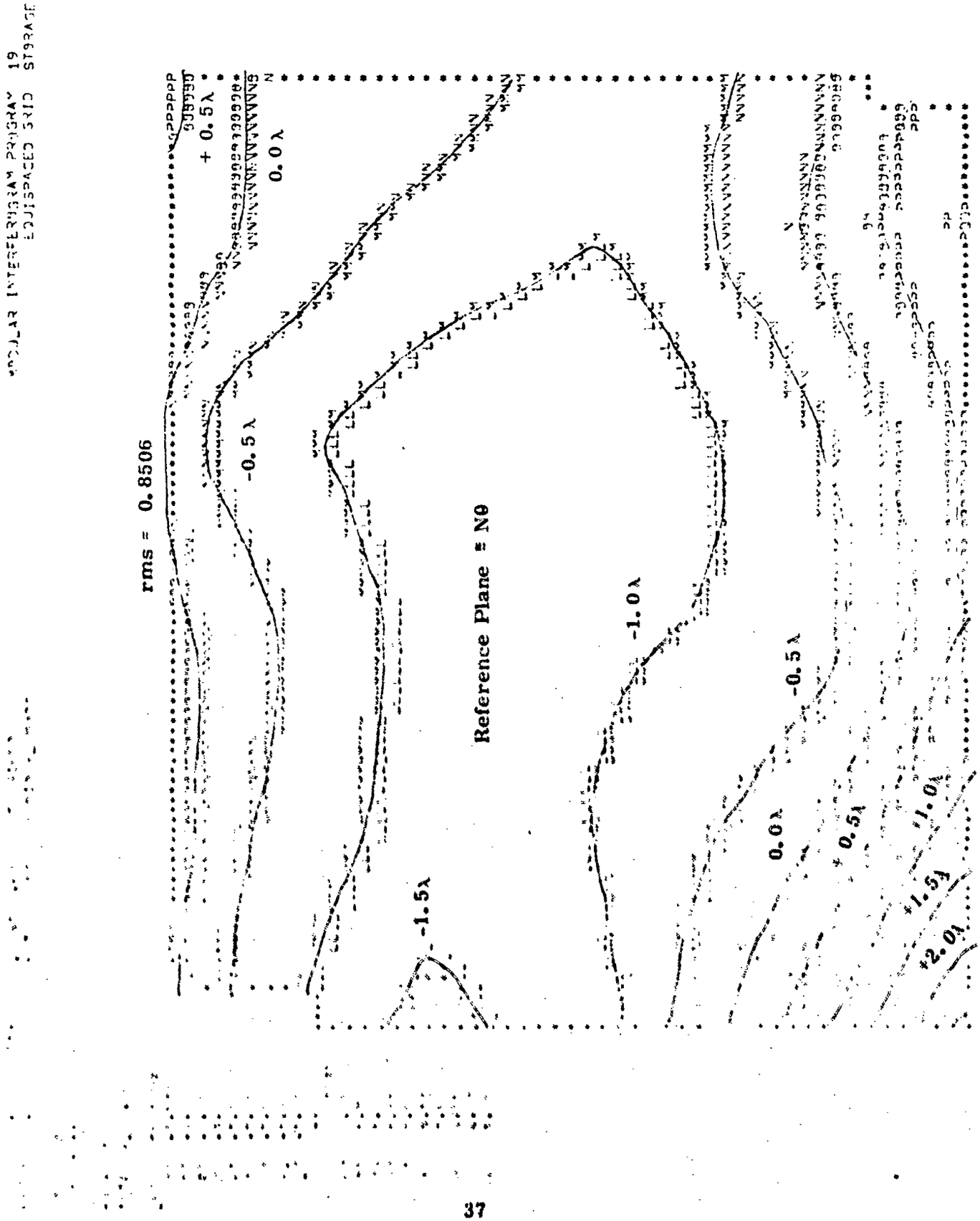

TRANSMITTED WAVEFRONT AT 10.6μm
FIGURE 16A

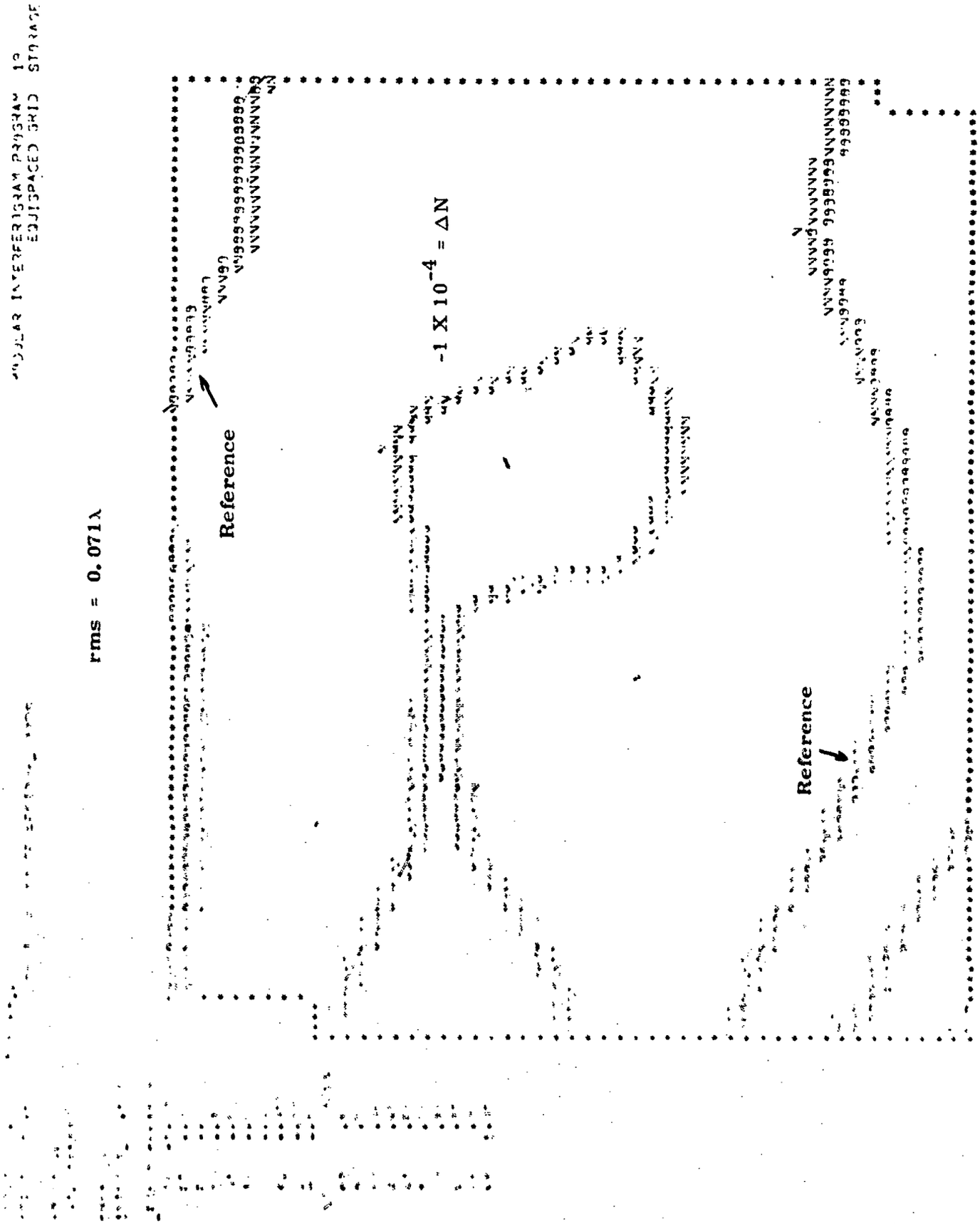

TRANSMITTED WAVEFRONT AT 0.9μm AT BEST FOCUS

FIGURE 17

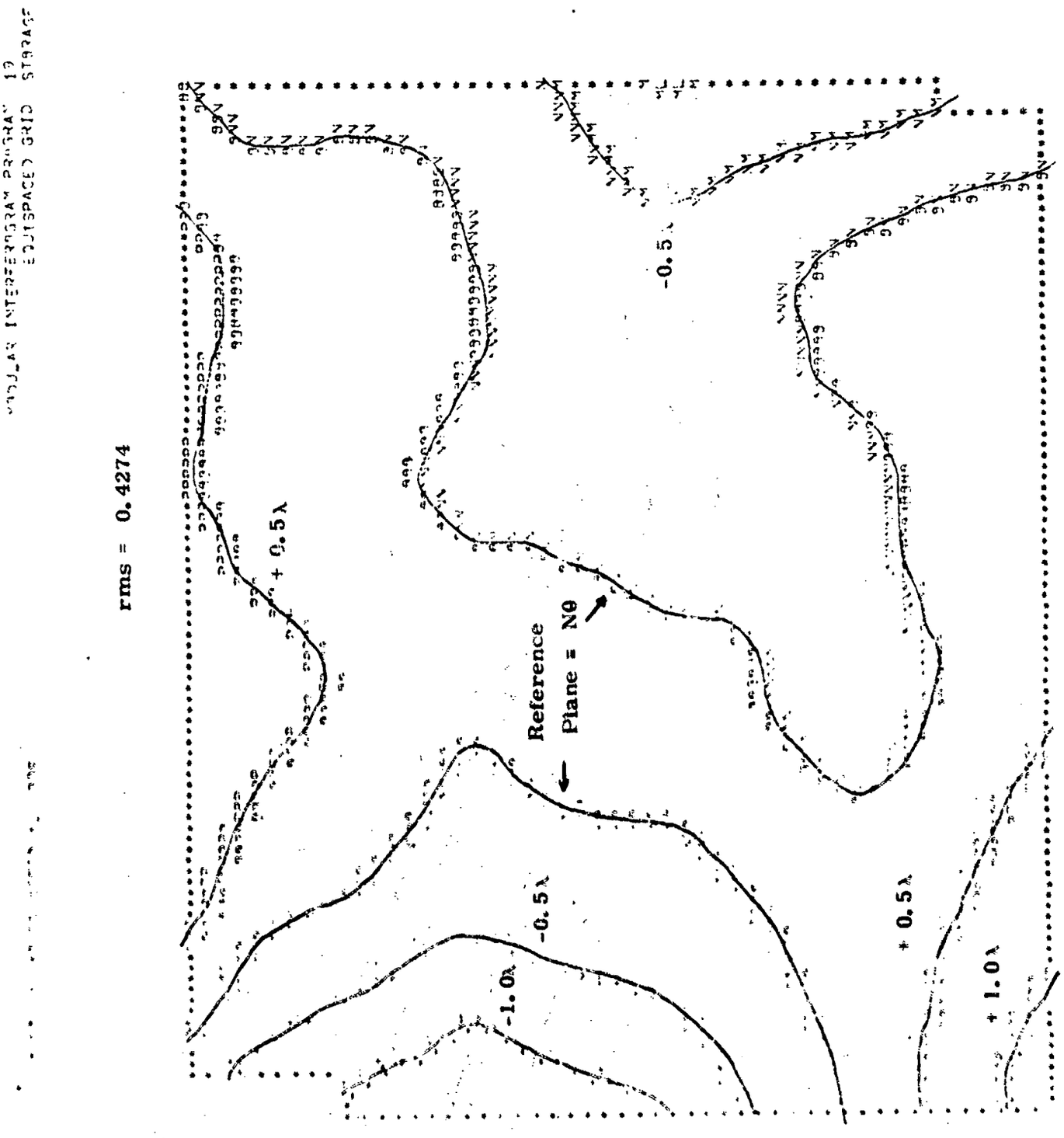

TRANSMITTED WAVEFRONT AT 10.6μm AT BEST FOCUS
FIGURE 17A

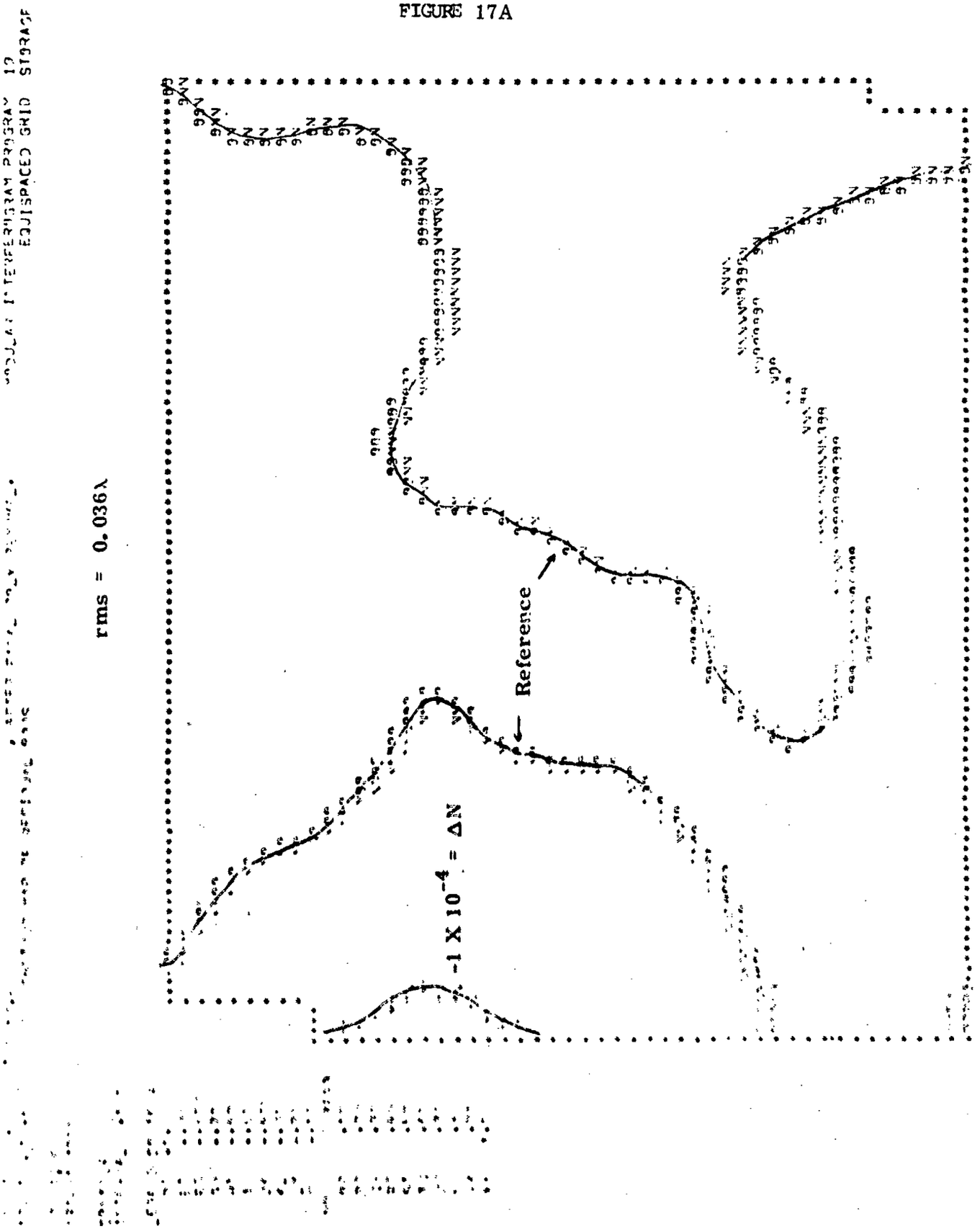

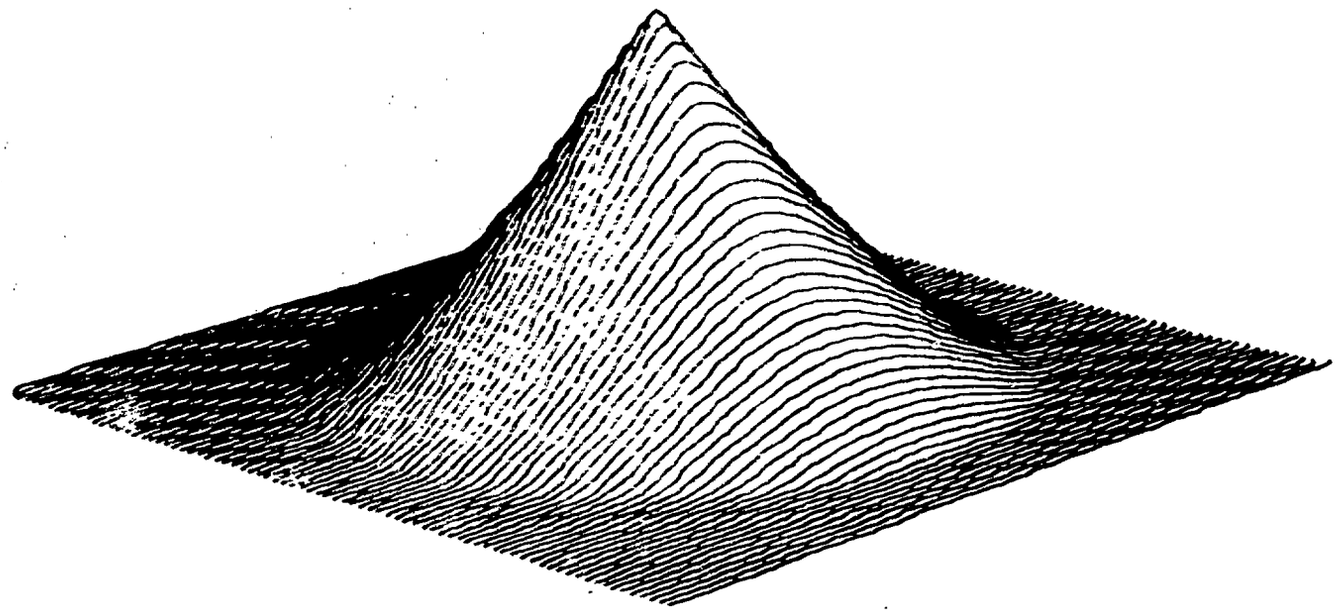

Fig. 18. MTF at 10.6 μm

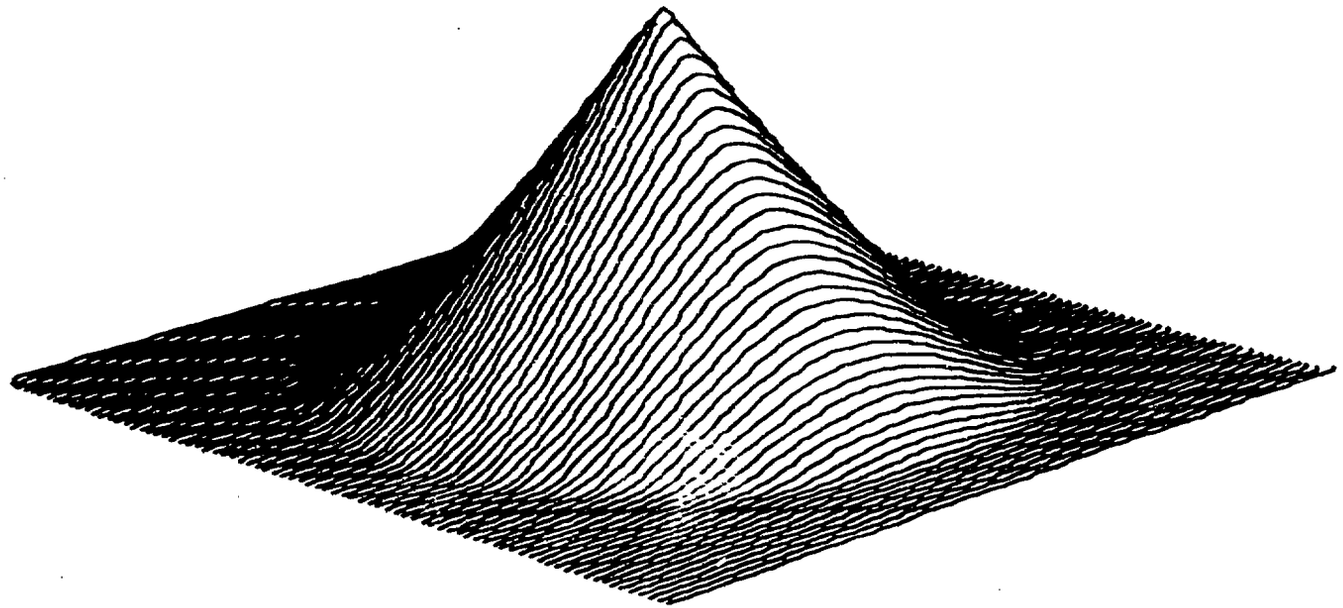

Fig. 19 MTF at 10.6 μm (Best Focus)

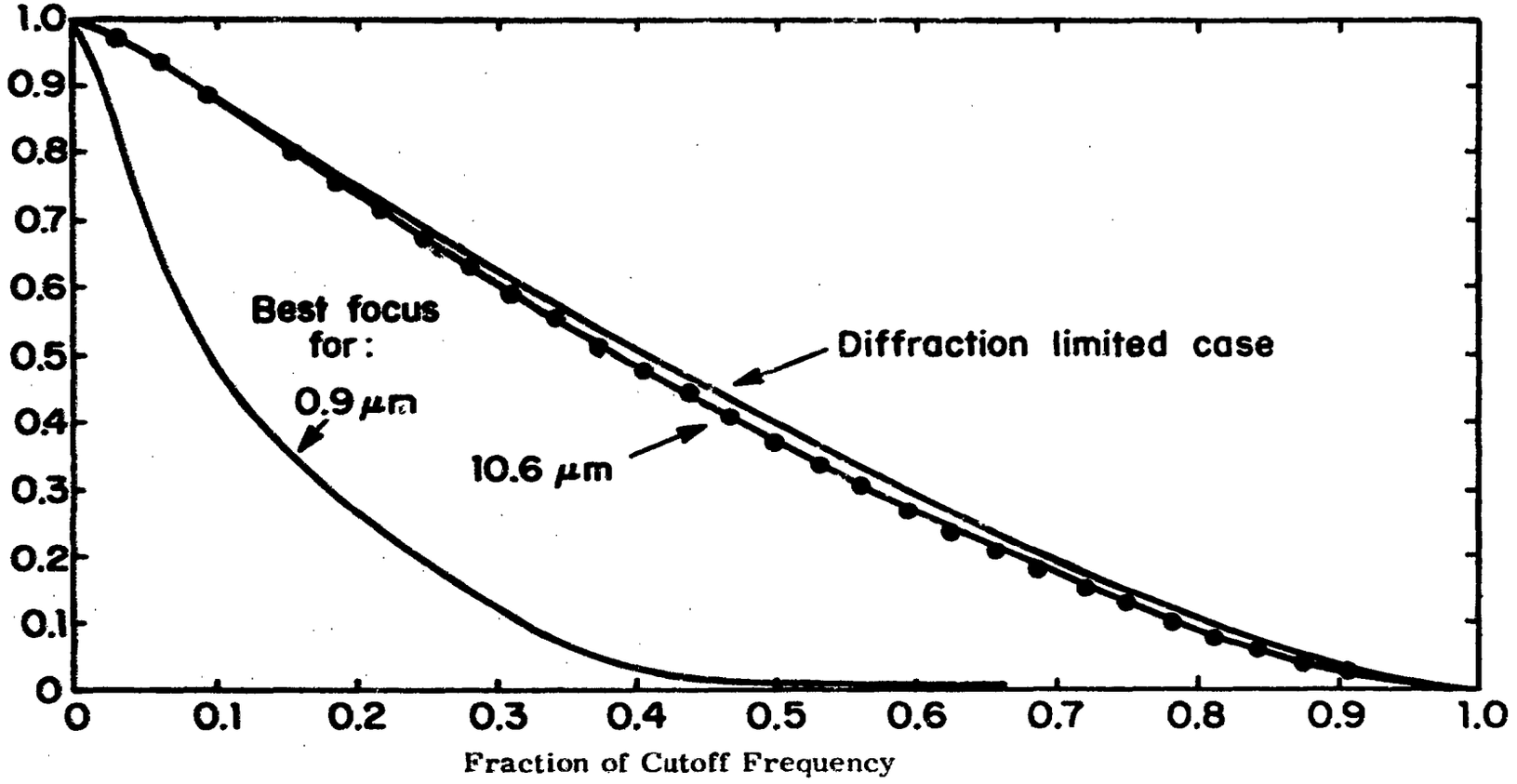

Fig. 20 Modulation Transfer Function at 0.9 μm and 10.6 μm

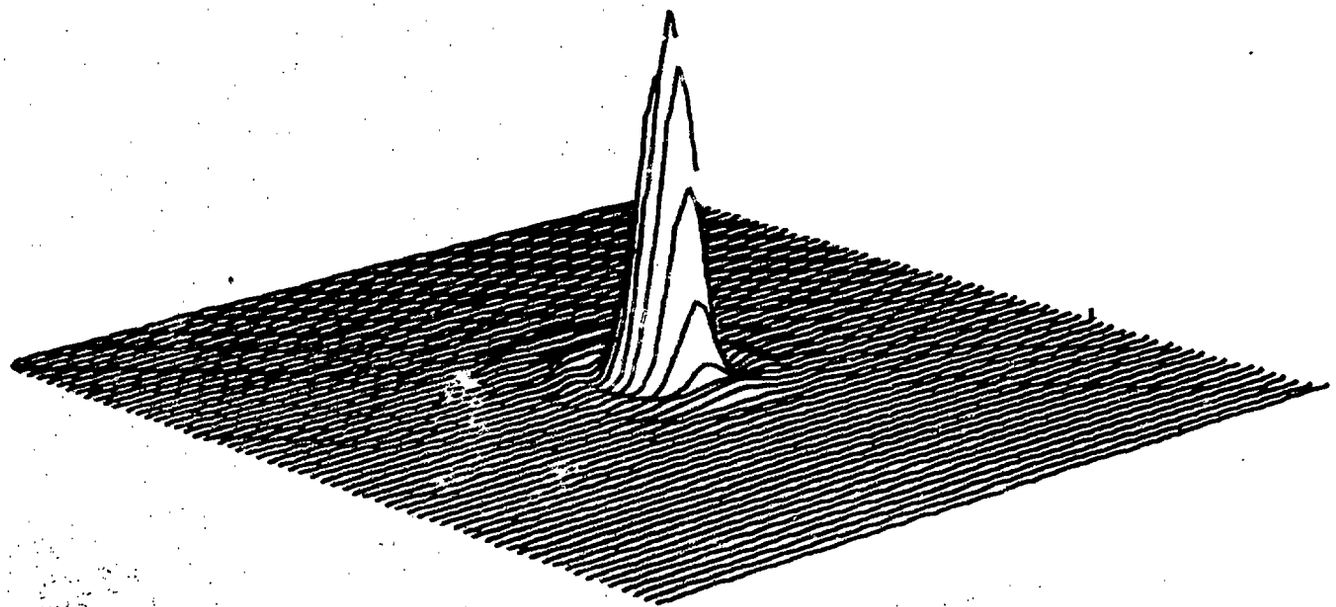

Fig. 21 PSF at 10.6 μm

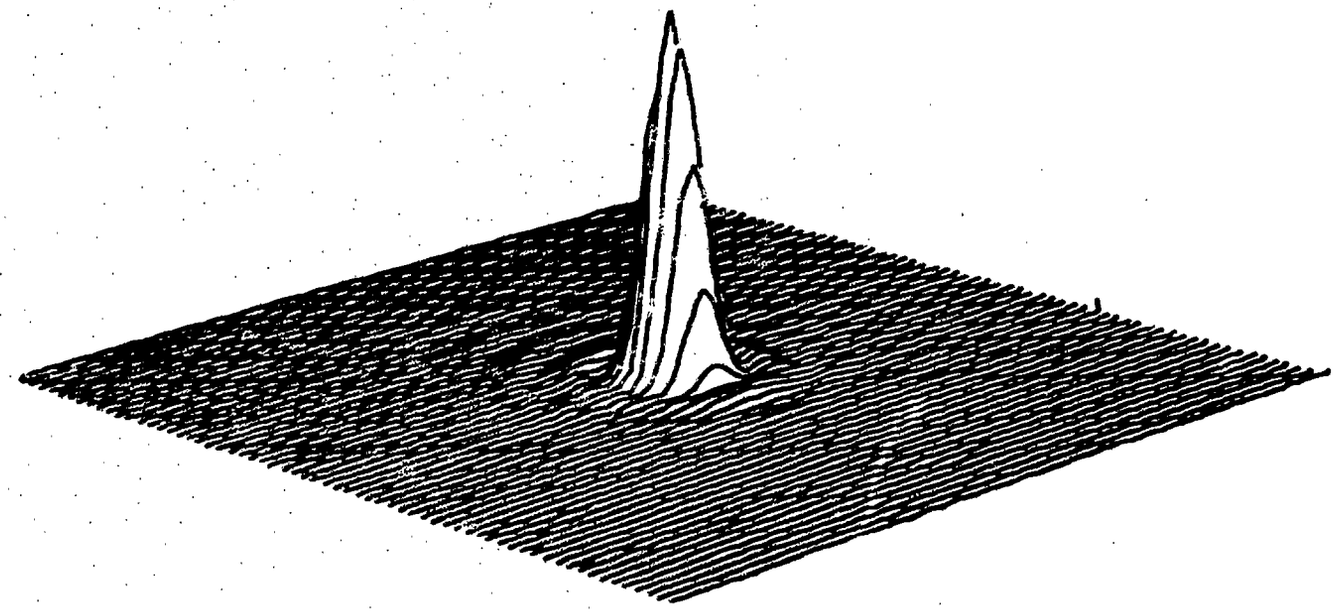

Fig. 22 PSF at 10.6 μm (Best Focus)

PBN-73-542

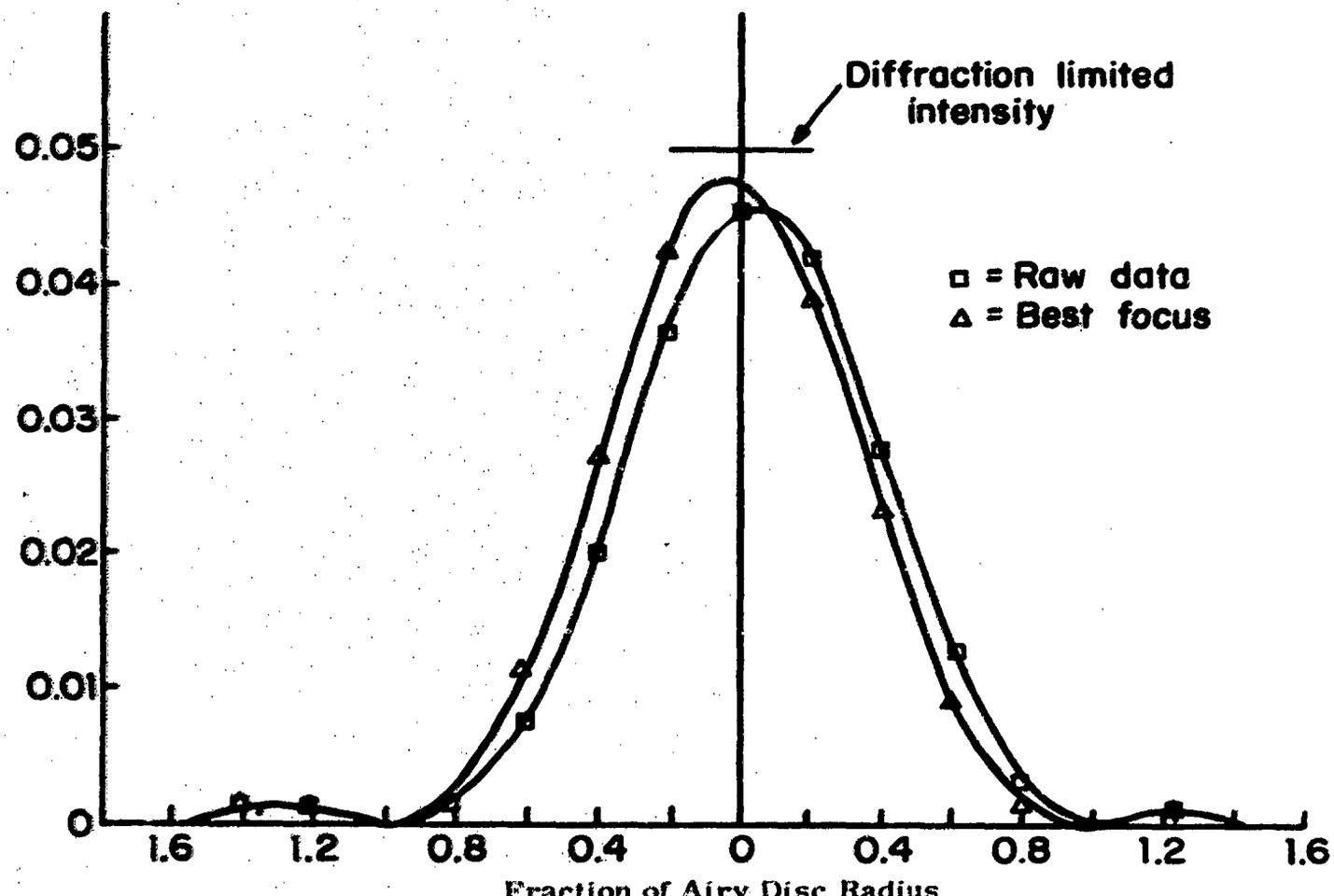

Fig. 23 Point Spread Function at 10.6 μm

d. Summary

The conclusion to be drawn from these interferometer measurements is that an essentially diffraction limited imaging can be expected in the passive i. r. band 8-11.5 μm. At shorter wavelengths the angular resolution will remain roughly equal to that obtainable in the 8-11.5 μm band, and will therefore fall away progressively from that predicted for a diffraction limited short wavelength system with a 4 in. aperture. This performance, however, is sufficient for use in known infrared and dual mode applications. It follows that the main problem with the use of CVD zinc sulfide is in the overall signal reduction due to residual scatter, and in the increased background levels that will degrade the performance of systems designed not for thermal sensing, but for active i. r. or passive sensing at wavelengths in the visible and near i. r. wavelength range. The latter uses will also be affected by the extrinsic absorption band between 0.4 and 0.9 μm. The first problem is one of process control, to minimize the occurrence of scatter bands. The extrinsic absorption can in fact be eliminated by annealing, by deposition at high temperatures, and possibly by the use of aliovalent additives. The problem is to find a corrective technique compatible with the deposition of a low-scatter, physically sound material.

SECTION V
CONCLUSIONS

The feasibility of utilizing the chemical vapor deposition process to fabricate large aperture size infrared windows of zinc sulfide was further demonstrated by depositing plate material whose nominal size was 14 × 20 in. This program addressed itself to eliminating visible-to-the-eye inclusions, reducing scatter in the visible, eliminating plate fracture and attaining a more uniform profile thickness over the desired area. Three of the problems addressed were solved, while the remaining one, scatter in the visible was reduced but not to the degree required.

Inclusions were eliminated by redesigning the CVD equipment and mandrel geometry. Fracture of plates during cooldown was avoided by the use of metal terminators at the ends of the mandrel. The thickness profile was improved by adjusting the velocity of the reactant gases as well as allowing the proper amount of premixing of the reactants prior to their introduction into the mandrel.

The one problem that was not satisfactorily resolved was scatter at visible wavelengths. Analysis of the material indicates that the scattering sites are micropores or in some cases finely dispersed particles of zinc that are entrapped in the material during deposition. The micropores are formed by the decomposition of zinc hydride during deposition, by the growth of a small percentage of a hexagonal phase of zinc sulfide along with the cubic phase of zinc sulfide, or by variations in the zinc usage rate during deposition.

Interferometer measurements on samples taken from large size plates indicates that diffraction limited imaging can be expected at all wavelengths and that even at 0.9 μm image degradation is slight. Angular resolution at all wavelengths will be degraded by less than 10 μradians by

transmission through one centimeter of CVD ZnS. The main problem with the use of this material is the overall signal reduction due to residual scatter, and in the increased background levels that will degrade the performance of systems designed not for thermal sensing, but for active i. r. or passive sensing at wavelengths in the visible and near i. r. wavelength range. The latter uses will also be affected by the extrinsic absorption band between 0. 4 and 0. 9 μm. Further improvements in the material for use in these wavelengths can be expected with the use of aliovalent additives as well as the use of other additives or process techniques that suppress the formation of scatter sites. Table II lists the current state-of-the-art properties of CVD ZnS.

TABLE II

TYPICAL PROPERTIES OF CVD ZnS

Density (gm/cc)	4.08
Hardness (Knoop 50 gm)	225
Flexural Strength (psi, 3-point loading)	15,200
Young's Modulus (psi)	10.8×10^6
Poisson's Ratio	0.33
Thermal Expansion (RT - 400°C $\times 10^{-6}$/°C)	7.48
Thermal Conductivity RT (cal. sec.$^{-1}$ C^{-1} cm^{-2} cm)	0.036
Specific Heat (25° - 95° C)(gm/cal/°C)	0.112
Electrical Resistivity (ohm-cm)	$\sim 10^{12}$
Total Absorption Coefficient @ 10.6 μm (cm^{-1})	0.22
Percent Transmission for 0.2 in. thickness at various wavelengths (μm)	
0.5 μm	10
0.7	46
1.0	58
2.5	69.5
5.0	71.5
8.0	72.5
9.0	72.5
10.5	68.5
11.0	61
11.5	60

DISTRIBUTION

No. of Copies	
2	DDC Cameron Station Alexandria, VA 22314
3	AFAL/TEL-1 (C. T. Ennis) Wright-Patterson AFB, OH 45433
1	Defense Ceramic Information Center Battelle Memorial Inst. Room 11-9021 505 King Avenue Columbus, OH 45201
1	AFAL/TSR Wright-Patterson AFB, OH 45433
1	2760th ABW/SSL Wright-Patterson AFB, OH 45433
1	Air University Library Maxwell AFB, AL 36112
1	Hq USAF (SAMID) Washington, DC 20330
1	AFAL/RSP-4 (Attn: Mr. M. Carr) Wright-Patterson AFB, OH 45433
1	Perkin-Elmer Co. Attn: E. Strouse 77 Danbury Road Wilton, CT 06897
1	General Electric Company Attn: E. L. Bartels P. O. Box 2143 Kettering Branch Dayton, OH 45429
1	Martin Marietta Corp. Attn: Mr. D. R. Maley P. O. Box 5837 Orlando, Florida 32805

No. of Copies	
1	Hughes Aircraft Company Aerospace Group Missile Systems Division Attn: Mrs. V. F. Olson Canoga Park, California
1	Texas Instruments Inc. Equipment Group Electro-Optics Division Attn: Mr. Bob Crossland P. O. Box 6015 Dallas, Texas 75222
4	ASD/ RWRS Attn: Lt. Col. James R. Wolverton SCANA Program Office Directorate of Recon/ Strike Projects Wright-Patterson AFB, OH 45433

UNCLASSIFIED

Security Classification

DOCUMENT CONTROL DATA - R & D

(Security classification of title, body of abstract and indexing annotation must be entered when the overall report is classified)

1 ORIGINATING ACTIVITY (Corporate author)	2a. REPORT SECURITY CLASSIFICATION
Raytheon Company Research Division Waltham, Massachusetts	UNCLASSIFIED
	2b. GROUP N/A

3 REPORT TITLE

Improved Large ZnS Windows

4 DESCRIPTIVE NOTES (Type of report and inclusive dates)

Final Technical Report, August 1972 to January 1973

5 AUTHOR(S) (First name, middle initial, last name)

Bernard A. diBenedetto, James Pappis, Anthony J. Capriulo

6 REPORT DATE	7a. TOTAL NO. OF PAGES	7b. NO. OF REFS
May 1973	50	0

8a. CONTRACT OR GRANT NO	9a. ORIGINATOR'S REPORT NUMBER(S)
F33615-73-C-1048	
b. PROJECT NO 6102	S-1559
c.	9b. OTHER REPORT NO(S) (Any other numbers that may be assigned this report) AFAL-TR-73-176
d.	

10 DISTRIBUTION STATEMENT

Distribution limited to U. S. Government agencies only; report contains test and evaluation information, May 1973. Other requests for this document must be referred to AFAL/TEI, Wright-Patterson AFB, Ohio.

11 SUPPLEMENTARY NOTES	12 SPONSORING MILITARY ACTIVITY
N/A	Air Force Avionics Laboratory Air Force Systems Command Wright-Patterson AFB, Ohio

13 The significance of this research and development program to the Air Force is the demonstrated feasibility of fabricating large infrared transmitting windows of zinc sulfide with good physical and optical characteristics by the chemical vapor deposition process. Plates approximately 1 ft. × 2 ft. with good transmitting properties in the 8-12 μm band were made and samples from these plates were submitted to the Air Force Avionics Laboratory for further evaluation.

Three major accomplishments of the program were: the elimination of visible-to-the-eye zinc inclusions, the elimination of plate fracture during cooldown from the deposition temperature, and the improvement of the as-deposited thickness profile. As a result of these improvements the cost of window blanks can be significantly reduced.

Interferometric measurements on samples taken from typical deposits indicate that diffraction limited imaging can be expected at all infrared wavelengths and that even at 0.9 μm image degradation is still slight. Angular resolution at all wavelengths will be degraded less than 10 μradians by transmission through 1 cm of the material, and is adequate for all known infrared systems applications. The main problem with the use of this material is in the overall signal reduction due to residual scatter, and in the increased background levels that will degrade the performance of systems designed not for thermal sensing but for active i. r. or passive sensing at wavelengths in the visible and near i. r. wavelength range. The latter uses will also be affected by the extrinsic absorption band between 0.4 and 0.9 μm. Improvement of the material for these applications may possibly be accomplished by use of aliovalent additives as well as by the use of additives that suppress the formation of scattering sites

DD FORM 1473

UNCLASSIFIED

Security Classification

14 KEY WORDS	LINK A		LINK B		LINK C	
	ROLE	WT	ROLE	WT	ROLE	WT
Reconnaissance						
Intrared transmission						
Zinc Sulfide						
Optical Windows						
MTF						